

INTRODUCTION TO SOLID-STATE NMR SPECTROSCOPY AND ITS  
APPLICATION TO THE STUDY OF SOILS AND RELATED SYSTEMS

Walter V. Gerasimowicz and Philip E. Pfeffer

TABLE OF CONTENTS

I.	General Principles of Solid-State NMR .....	266
	A Introduction .....	266
	B. Basis of Nuclear Spin Interactions in Solids .....	266
	C. Solid-State NMR Methodology .....	268
	1. Cross-Polarization of Dilute Spins .....	268
	2. High-Power Proton Decoupling .....	271
	3. Magic Angle Spinning .....	273
II.	Direct CPMAS Measurements of Whole Soils .....	274
	A. Experimental Conditions — Spin Dynamic Considerations .....	275
	1. NMR Spectrometer Settings .....	275
	2. Degree of Cross-Polarization Enhancement .....	275
	3. Model Response System for Soils, Mucks, Sludges, and Humic and Fulvic Systems .....	278
	4. Humic Substances .....	282
	5. Soil/Plant Components: Lignin-Carbohydrates — Interrupted Decoupling .....	292
	B. Some Other Nuclei in CPMAS Studies of Soils .....	298
	1. <sup>31</sup> P NMR Studies in Soil Systems .....	298
	2. <sup>15</sup> N NMR Studies in Soil Systems .....	299
	3. High-Resolution Solid-State Proton NMR of Soil Materials .....	301
	4. Oxygen-17 and Other Nuclei .....	301
III.	Conclusions .....	305
	References .....	305

## I. GENERAL PRINCIPLES OF SOLID-STATE NMR

### A. Introduction

Over the past 25 years, high-resolution liquid-state NMR has become the most widely utilized technique employed in the elucidation of molecular structure, identification of chemical species, and in the study of nuclear spin dynamics. NMR spectroscopy (as seen in the other chapters of this book) is an invaluable tool for the investigation of phenomena, such as chemical shift and proton coupling in the liquid or solution state. Due to the fact that the experimentalist can obtain high-resolution spectra, one can observe weak interactions, such as those associated with spin-spin coupling and with the chemical shift. Such interactions are a reflection of the local nuclear spin environment, and may be used as a diagnostic probe of that phenomenological level. However, NMR spectroscopists have continued to cope with several serious limitations. Lack of NMR sensitivity due to sample size limitation is being overcome by increases in magnetic field strength, electronic development, and computer (data processing) technology. Many scientists viewed the requirement (until recently) of liquid samples as the greatest limitation with respect to NMR analysis. Although solid-state physicists have conducted wide-line studies since the early days of NMR, these results have been of little practical interest to chemists, biochemists, agricultural, and soil scientists. Developments over the last few years have resulted in a dramatic and ever-expanding growth in this area of research.

This chapter is written with several purposes in mind. We intend to provide the reader with a concise overview of the practical limitations as well as the major problems associated with solid-state NMR research. Our emphasis will center upon  $^{13}\text{C}$  cross-polarization magic angle spinning ( $^{13}\text{C}$ -CPMAS) with other examples as appropriate. However, many of the solutions applied to the procurement of solid-state carbon spectra can be analogously utilized in other heteronuclear pulse experiments of this type. Most of the subject matter is too complex to be fully discussed either theoretically or mathematically within the intended scope of this volume. Literature references will be cited so that the reader can later pursue various areas of personal interest in depth. Selected topics and papers (but not exhaustive) are presented to give the agricultural scientist examples from the literature which may stimulate an awareness for the vast potential, which is as yet untapped, in this "fertile field" of spectroscopy.

Obviously, solid-state NMR is having an enormous impact on agricultural science from the standpoint of the study of agricultural materials, their structure, polymeric properties, structure-function relationships, and chemical and biological properties which only represent a partial list of the areas which could be mentioned. Furthermore, several profound reasons could be given for the study of agricultural substances in the solid state. The solid may be insoluble or intractable. Additionally, the scientific question of interest may concern the properties of the material in the solid state itself. One can never be absolutely certain that data obtained while molecules are in solution is necessarily a reflection of the solid state. Molecular structure may change markedly when the species is in different phases. High-resolution NMR in the solid state can be used (in certain situations) to confirm the validity of X-ray structural determinations, conformations, and molecular configurations. The technique is non destructive. The sample utilized in the solid-state NMR study is retained intact and unmodified, and has not been subjected to solvent interactions. Valuable and rare samples are thus preserved and do not require extensive recovery from or removal of solvent.

By convention  $^1\text{H}$  (abundant spin) will be designated as I and  $^{13}\text{C}$  (rare spin) will be designated as S. At times the IS notation will be employed to remind the reader of the generality of this discussion *i. e.*, the fact that we are discussing spin systems in which two different spin species are present or heteronuclear interactions are being treated.

### B. Basis of Nuclear Spin Interactions in Solids

A summary of the basic nuclear spin interactions which occurs in solids is depicted in Figure 1. Formal and detailed descriptions of the physics and quantum mechanics may be found in the

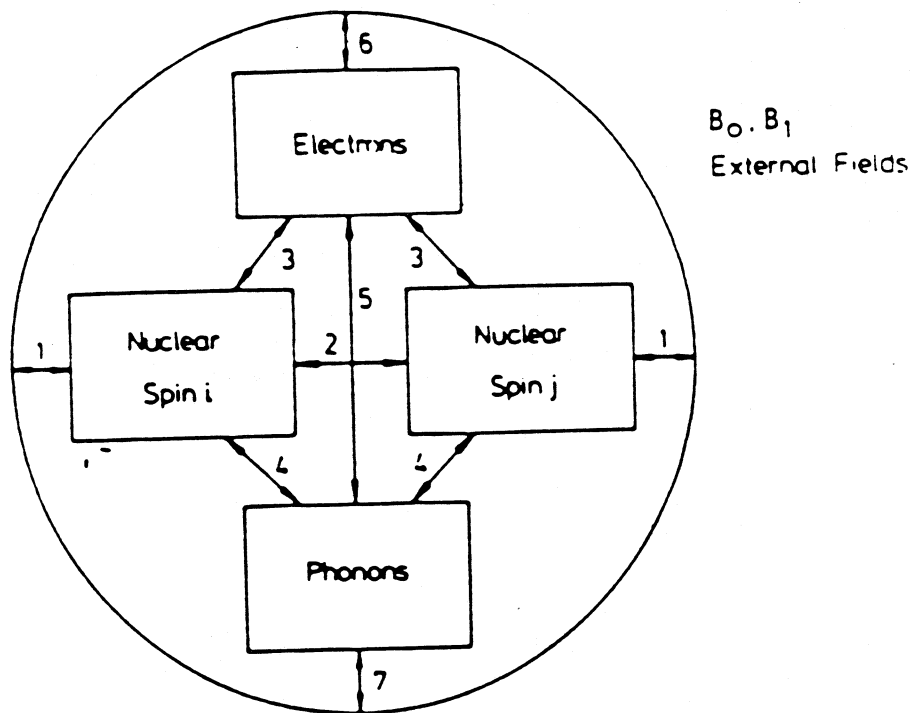


FIGURE 1. The sevenfold way a nuclear spin system can interact with its surrounding. (1) Zeeman interaction of spins, (2) direct spin interactions, (3) nuclear spin-electron interaction and indirect spin interaction, (4) direct spin-lattice interaction, (3 to 5) indirect spin lattice interaction via electrons, (3 to 6) shielding and polarization of nuclear spins by electrons, and (4 to 7) coupling of nuclear spins to sound fields, etc. (From Mehring, M., *High Resolution NMR in Solids*, 2nd ed., Springer-Verlag, Berlin, 1983. With permission.)

excellent texts of Mehring<sup>1</sup>, Slichter,<sup>2</sup> Haeblerlein,<sup>3</sup> Gerstein and Dybowski,<sup>4</sup> and of course in Abragam.<sup>5</sup> The nuclear spin interactions can be expressed first in terms of the effects between internal and external magnetic fields ( $B_0$  and  $B_1$ ).

$$\mathcal{H} = \mathcal{H}_{\text{ext}} + \mathcal{H}_{\text{int}} \quad (1)$$

where

$$\mathcal{H}_{\text{ext}} = \mathcal{H}_0 + \mathcal{H}_1 \quad (2)$$

$\mathcal{H}_0$  and  $\mathcal{H}_1$  are the Hamiltonian operators which represent the Zeeman interactions corresponding to the internally induced fields due to  $B_0$  and  $B_1$ . The internal Hamiltonian for the interaction of two different spins (I and S) with corresponding magnetogyric ratios of  $\gamma_I$  and  $\gamma_S$  is shown in equation (3):

$$\mathcal{H}_{\text{int}} = \mathcal{H}_{\text{II}} + \mathcal{H}_{\text{SS}} + \mathcal{H}_{\text{IS}} + \mathcal{H}_Q + \mathcal{H}_S + \mathcal{H}_L \quad (3)$$

$\mathcal{H}_{\text{II}}$  and  $\mathcal{H}_{\text{SS}}$  represent direct and indirect interactions among the various spins (path 2 and 3) as shown in Figure 1. Paths 2 and 3 are also involved in the IS interactions with the corresponding  $\mathcal{H}_{\text{IS}}$  operator.  $\mathcal{H}_Q$  is the quadrupolar operator. The shielding Hamiltonians are depicted by  $\mathcal{H}_S$ , i.e., Knight and chemical shifts (paths 3 and 6 in the Figure).  $\mathcal{H}_L$  represents the spin-lattice interactions as seen in paths 3, 4, and 5 of Figure 1. A summary of the other terms in Equation 3 and a tabulation of the explicit forms of the Hamiltonian are shown in Table 1.<sup>1</sup>

**Table 1**  
**INTERACTION HAMILTONIANS**

Interaction	Form of the Hamiltonian
Chemical shift	$\mathcal{H}_c = \gamma I \cdot \vec{\sigma} \cdot B_0$
Dipole-dipole	$\mathcal{H}_D = \sum_{i < j} \hbar \gamma_i \gamma_j r_{ij}^{-3} \left( I_i \cdot I_j - \frac{3(I_i \cdot r_{ij})(I_j \cdot r_{ij})}{r_{ij}^2} \right)$ $\mathcal{H}_D = \sum_{i < j} I_i \cdot \vec{D} \cdot I_j$ $D_{\alpha\beta} = \hbar \gamma_i \gamma_j r_{ij}^{-3} (\sigma_{\alpha\beta} - 3e_\alpha e_\beta)$ $\alpha, \beta = x, y, z; e_\alpha: \alpha\text{-component of the unit vector along } r_{ij}$
J-coupling	$\mathcal{H}_J = \sum_{i \neq j} I_i \cdot \vec{J} \cdot I_j$
Spin-rotation	$\mathcal{H}_{CR} = \sum_i I_i \cdot \vec{C}_i \cdot J$
Quadrupole	$\mathcal{H}_Q = \frac{eQ}{2I(2I - 1)\hbar} I \cdot \vec{V} \cdot I$ $\vec{V} = \{V_{\alpha\beta}\}; \alpha, \beta = x, y, z$

### C. Solid-State NMR Methodology in Solids

Attempts to obtain solid-state  $^{13}\text{C}$  NMR spectra by using ordinary pulse Fourier transform techniques and instrumentation as employed for routine liquid samples will normally not even result in a spectrum which can be detected. The major (although not the exclusive) reason for the lack of resolution in the spectra of typical solids is the dipole-dipole interaction exerted by protons. Furthermore, rare spins are generally dipolar-coupled to abundant spins in the solid state. Due to their low natural abundance (1.1% in the case of  $^{13}\text{C}$ ), the signal which can be detected from a single experiment is generally small, and signal averaging must be implemented. The repetition rate, however, is dependent upon the time (the  $^{13}\text{C}$  spin-lattice relaxation time) necessary for the  $^{13}\text{C}$  nuclei to recover (for the most part) to their equilibrium state and orientation after being subjected to an rf pulse at or near the resonance frequency of the nuclei. Chemical shift anisotropy (CSA) also results in line broadening. The chemical shift observed for a nucleus is a function not only of its identity, but also depends on its orientation within the molecule relative to the magnetic field. As such, in powders and solid samples where isotropic motion and rapid and random tumbling is not present (as in solutions where sharp lines are seen due to rapid motional averaging), a broad band of resonance frequencies is observed for individual carbon types which can be as broad as the typical frequency range over which  $^{13}\text{C}$  is normally observed.

#### 1. Cross-Polarization of Dilute Spins

Due to their low natural abundance, rare spins do not exhibit significant homonuclear dipole-dipole interactions. This advantage is reduced by the inherent low signal-to-noise which is due to the low population of nuclei which can be observed. One can attempt to enrich the sample isotopically. Such procedures may be costly and may affect the characteristics of the sample

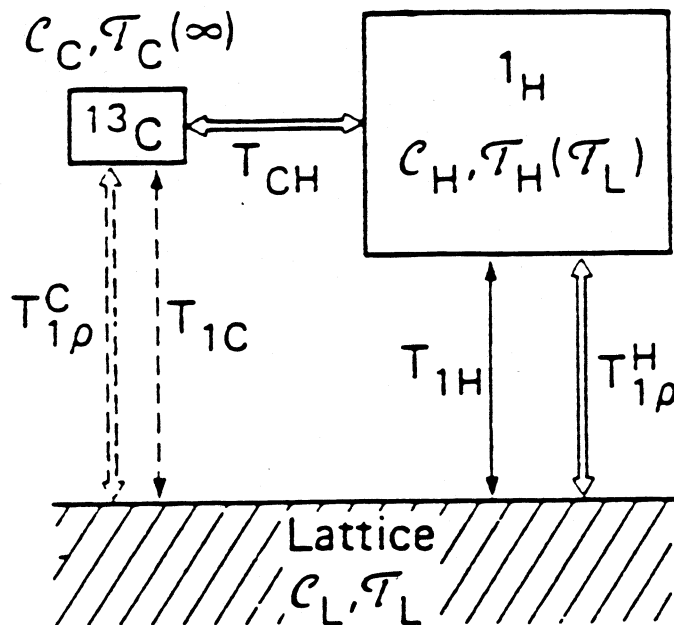


FIGURE 2. Large  $^1\text{H}$ , small  $^{13}\text{C}$ , and infinite lattice reservoir, characterized by a heat capacity,  $C$  (vide infra), and temperature  $T$ . Temperatures in parentheses are those at the start ( $t = 0$ ) of the CP sequence. (From Yannoni, C. S., *Acc. Chem. Res.*, 15, 201, 1982. With permission.)

under study. Other methods have been devised which permit observation of dilute nuclei in a solid by taking advantage of the strong dipole-dipole interactions among abundant and rare spins. This process is commonly referred to as cross-polarization (CP) or polarization transfer. The history of polarization transfer can be traced back to the 1950s and the 1960s.<sup>6-10</sup> Several research groups demonstrated that they could detect communication between spins in a spin-locked system which was externally perturbed. Hartmann and Hahn<sup>6</sup> were able to detect rare spins by means of a double resonance experiment.

The basic manner in which CP is carried out in order to observe  $^{13}\text{C}$  nuclei at natural abundance in the presence of an abundant proton spin population depends upon spin temperature. When a solid organic sample experiences a magnetic field ( $H_0$ ), the individual protons comprising the sample will align parallel and antiparallel to  $H_0$ . They will populate Zeeman energy levels with energies of  $\pm(\gamma_H/2\pi)H_0/2$ . These energy levels correspond to spin alignments which are either parallel or antiparallel to  $H_0$ . The protons will undergo mutual spin flips by exchanging energy with the lattice until a state of internal equilibrium is attained ( $\sim 100 \mu\text{s}$ ). Upon reaching this equilibrium state, they can be treated as a thermodynamic reservoir which requires several  $T_{1H}$ 's (proton spin-lattice relaxation times) to equilibrate with the lattice at some temperature  $T_L$ .<sup>11</sup> This process is depicted in Figure 2. At this point, the proton magnetization may be defined as follows:

$$M_{0H} = C_H H_0 / T_L \quad (4)$$

$$E = C_H H_0^2 / T \quad (5)$$

$$\mathcal{L} = (C_H H_0^2 / T^2) + \text{constant term} \quad (6)$$

$E$  is the energy,  $\mathcal{L}$  is the entropy, and  $C_H$  is the Curie constant defined in Equation 7 as:

$$C_H = N_H \gamma_H^2 \hbar^2 / 4k \quad (7)$$

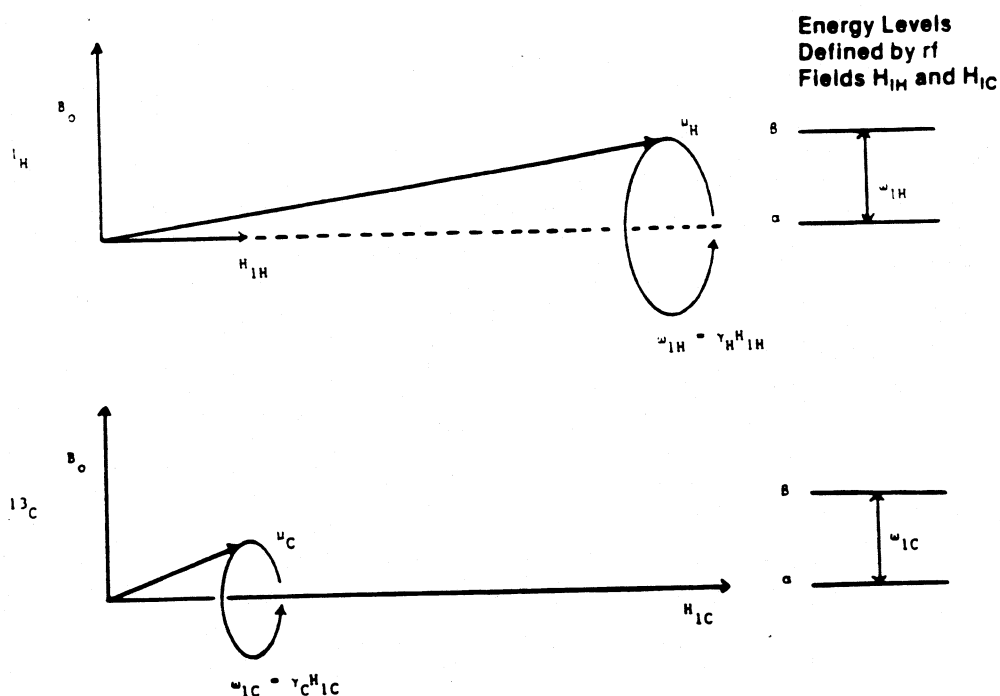


FIGURE 3. Matched rotating frame energy levels for  $^1\text{H}$  and  $^{13}\text{C}$  spin species during the Hartmann-Hahn condition. In the diagram,  $H_{1\text{H}}$  and  $H_{1\text{C}}$  are applied rf fields,  $\gamma_{\text{H}}$  and  $\gamma_{\text{C}}$  are the respective gyromagnetic ratios, and  $\omega_{1\text{H}}$  and  $\omega_{1\text{C}}$  are the energy levels (in units of  $\text{rad s}^{-1}$ ) induced by the rf fields. Since  $\omega_{1\text{H}} = \omega_{1\text{C}}$  under the match condition, efficient CP can occur. (From O'Donnell, Bartuska, V. J., Palmer, A. R., and Sindorf, D. W., *Am. Lab.*, 104, 1986. With permission.)

$N_{\text{H}}$  is the number of proton spins and  $k$  is the usual Boltzmann constant.<sup>12</sup> Not only can the spin system be considered a reservoir, but also the S spin system can form a reservoir both of which are in contact with one another and with the lattice as well. The rate at which polarization is transferred from the I to the S reservoir is described kinetically by the cross-relaxation time  $\Gamma_{\text{IS}}$  or in this case  $T_{\text{CH}}$ .

Three steps are involved in the CP process. The first step involves cooling or reduction of the S spin temperature. The magnetization of the carbon nuclei is rather small initially due to the fact that  $T_{\text{C}}$ , the carbon spin temperature is large:

$$M_{\text{OC}} = C_{\text{C}}H_0/T_{\text{C}} \quad (8)$$

and

$$C_{\text{C}} = N_{\text{C}}\gamma_{\text{C}}^2\hbar^2/4k \quad (9)$$

where  $C_{\text{C}}$  is the Curie constant associated with the  $^{13}\text{C}$  nuclei and the other terms are defined analogously to Equation 7 above. In order to actually transfer polarization, thermal contact is established between the I and S spin reservoirs by means of applying a spin lock in the rotating frame. The S spins are first irradiated on resonance and the rf field is adjusted until the conditions in Equations 10 and 11 are fulfilled:

$$\gamma_{\text{H}}H_{1\text{H}} = \gamma_{\text{C}}H_{1\text{C}} \quad (10)$$

$$\omega_{\text{H}}^{\text{eff}} = \omega_{\text{C}}^{\text{eff}} \quad (11)$$

These equations define the Hartmann-Hahn match and are further illustrated by Figure 3.<sup>6,13</sup>

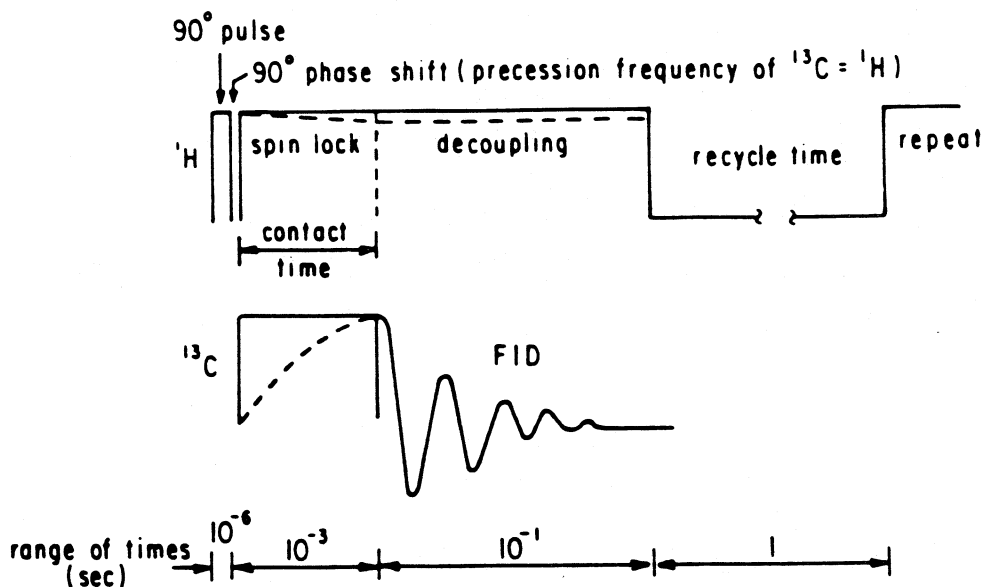


FIGURE 4.  $^{13}\text{C}$  solid-state CP sequence. (From Pfeffer, P. E., *J. Carbohydr. Chem.*, 3, 613, 1984. With permission.)

Therefore, an efficient mechanism has been established for magnetization transfer between the  $^1\text{H}$  and  $^{13}\text{C}$  reservoirs. Accordingly, as seen in Equation 8, the  $^{13}\text{C}$  spin temperature is reduced, and the  $^{13}\text{C}$  nuclear magnetization ( $M_{0c}$ ) increases. The process is depicted schematically in Figure 4 during the contact time (CT) period. Typical time regimes are also shown. Furthermore, the repetition rate of the experiment is now governed by the shorter  $^1\text{H}$  relaxation time (ca. 0.3 to 1.0 s), rather than by the much longer  $^{13}\text{C}$  relaxation time. Therefore, signal averaging and repetition of the basic experiment are much more efficient. Due to the CP process,  $^{13}\text{C}$  magnetization is enhanced by a factor of ca. 4 over that observed by natural relaxation mechanisms. In summary, Figure 4 depicts:

1. Establishment of I spin polarization in  $H_0$
2. Spin-locking of I spins along  $H_1^I$
3. Establishment of I and S spin contact via the Hartmann-Hahn matching condition
4. Turning off  $H_1^S$
5. Recording S-spin FID
6. Repeating sequence n times

## 2. High-Power Proton Decoupling

Proton dipolar broadening of  $^{13}\text{C}$  resonances in solids can be removed by means of high-power decoupling techniques. The protons are irradiated at their Larmor frequency. Effectively this irradiation stirs up the proton spins and eliminates the influence of the proton dipolar interaction on the  $^{13}\text{C}$  nuclei. The experiment is exactly analogous to scalar decoupling of protons in the liquid state, but requires much higher power. Dipolar couplings in a solid may be several thousand Hz as opposed to the much smaller J couplings found in the liquid state. Therefore, in order to effectively decouple protons in solids,  $^1\text{H}$  irradiation fields and power requirements are orders of magnitude larger (12 to 18 G) than those employed in liquids. Decoupling is normally carried out throughout the spin-locking and acquisition of the FID (Figure 4). Note the spectrum in Figure 5A where powdered crystalline sucrose is examined under solution state conditions as compared with Figure 5B where high-power proton decoupling is employed.<sup>14</sup> Although little detail is evident, some signal is beginning to emerge in Figure 5b.

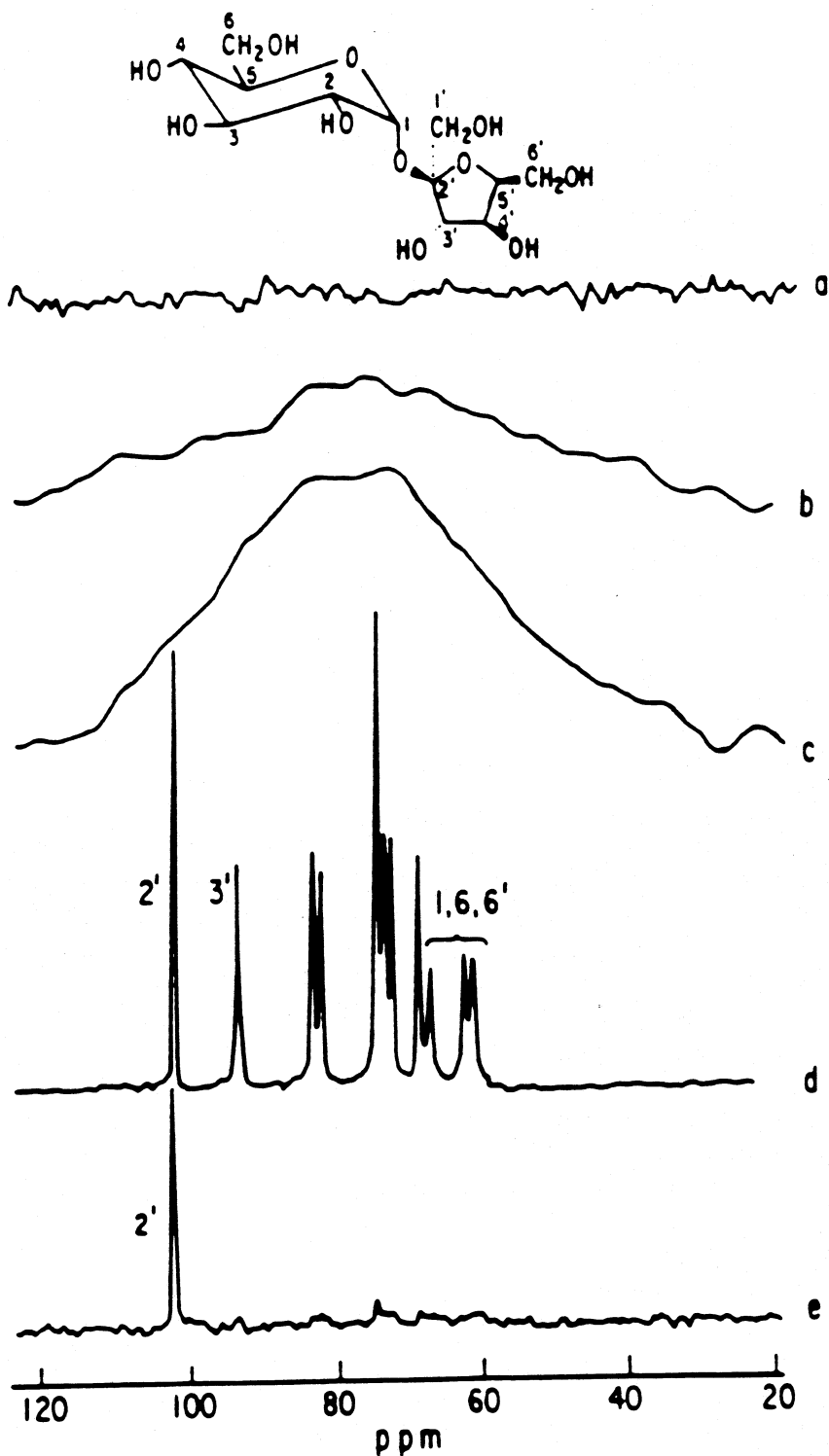


FIGURE 5. The 15-MHz  $^{13}\text{C}$  solid-state spectra of powdered crystalline sucrose taken under the following experimental conditions: (a) solution spectrum conditions.  $50^\circ$  pulse angle, 8-s pulse delay, and 5-kHz proton decoupling; (b) same conditions as a except with high-power decoupling of 45 kHz; (c) same as b except with proton-carbon CP, CT of 2 ms; (d) same as c except sample was spun at 2.0 kHz at the magic angle of  $54.7^\circ$ ; and (e) same as d except a 40- $\mu\text{s}$  delay without decoupling was inserted into the pulse sequence following the CT. (From Pfeffer, P. E., *J. Carbohydr. Chem.*, 3, 613, 1984. With permission.)

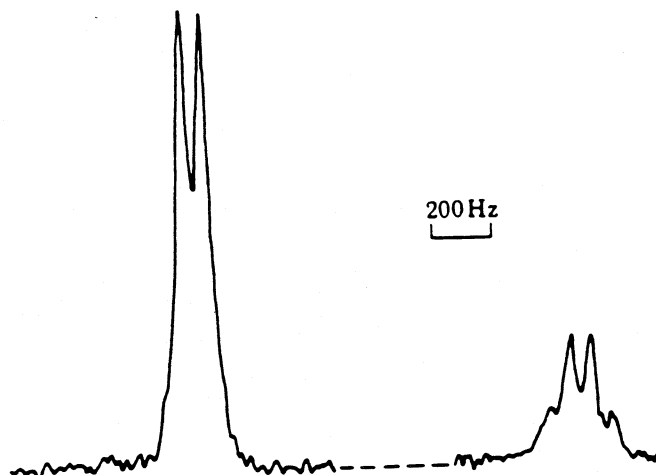


FIGURE 6.  $^{31}\text{P}$ -NMR spectrum in polycrystalline  $\text{P}_2\text{S}_5$  at 420 K (melting point 446 K). The spectrum is strongly narrowed by molecular motion in the solid and displays an  $\text{AB}_3$  type fine structure. (From Andrew, E. R., *Philos. Trans. R. Soc. London, Ser. A*, 299, 505, 1981. With permission.)

### 3. Magic Angle Spinning

The two techniques mentioned above (CP and high-power dipolar decoupling) would only provide limited insight(s) into the spin dynamics of solids if magic angle spinning (MAS) did not further increase the resolution seen in solid state NMR spectra. Most agricultural materials are intractable solid powders. Note in Figures 5b and 5c that high-power decoupling alone or CP does not appreciably enhance resolution where structural detail similar to liquid state spectra can be obtained. Complex powder spectra are much broader than those seen for liquids due to the overlap of many resonances. An excellent example of this phenomenon is provided in the case of the water molecule. The typical proton NMR line width of water at room temperature is on the order of 0.1 Hz or less. The line width of ice at low temperatures is approximately six orders of magnitude larger or about  $10^5$  Hz. This behavior has been well studied and is due to static anisotropic nuclear interactions in the solid state. In a liquid, rapid and random tumbling of the molecules averages out this anisotropy, and it is removed from the spectrum resulting in the nice sharp resonances one is accustomed to seeing. In some limited cases, sufficient motion is present in solids to result in NMR line narrowing. Figure 6 depicts such an example. An  $\text{AB}_3$  in the  $^{31}\text{P}$  spectrum could be resolved in the solid. The doublet was attributed to the three basal phosphorus nuclei in the molecule and the quartet to the apical nucleus.<sup>16,17</sup>

In most cases, however, sufficient motion is not present in solids to average the dipolar interactions. One alternative to this problem, MAS, was first introduced by Lowe and Andrew et al.<sup>18,21</sup> Effectively, one can emulate nature by mechanically imposing motion on the nuclei. Andrew's early studies also indicate that MAS affects other spin interactions, such as the chemical shift.<sup>21</sup> The combination of high power decoupling, CP, and MAS for rare spins was first shown by Schaefer et al.,<sup>22,23</sup> and for abundant spins by Gerstein.<sup>24</sup> Because of these developments, modern commercial spectrometers used for solid-state work are normally equipped with MAS capabilities.

The truncated dipolar Hamiltonian,  $\mathcal{H}_d$ , for all nuclear spin pairs in a solid is defined as

$$\mathcal{H}_d = \sum_{i < j} 1/2 \gamma_i \gamma_j \hbar^2 r_{ij}^{-3} (I_i \cdot I_j - 3I_{iz} I_{jz}) (3\cos^2 \theta_{ij} - 1) \quad (12)$$

In this equation,  $r_{ij}$  is the internuclear displacement,  $\theta_{ij}$  is the angle between the internuclear vector  $r_{ij}$  and the Zeeman field  $H_0$ , and the remaining terms are defined as previously specified. The geometry of the MAS experiment is shown in Figure 7.<sup>15</sup> The broadening due to chemical

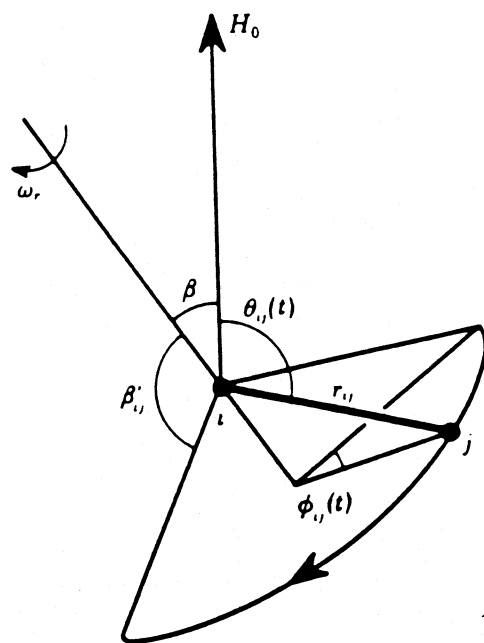


FIGURE 7. Diagram illustrating the motion of a typical internuclear vector  $r_{ij}$  when a solid is rotated with angular velocity  $\omega_r$  about an axis inclined at angle  $\beta$  to  $H_0$ . (From Andrew, E.R., *Philos. Trans. R. Soc. London, Ser. A.* 299, 505, 1981. With permission.)

shift anisotropy is eliminated (for the most part) by spinning at the "magic angle" of  $54.7^\circ$  with respect to  $H_0$  (Figure 7). This is the angle which causes the function  $(3\cos^2\theta_{ij} - 1)$  to vanish (Equation 12) and  $H_d = 0$ .

A summary of solution vs. high-resolution solid-state NMR spectroscopy is shown in Table 2.<sup>25</sup> Proper execution of the CPMAS experiment results in the spectrum shown in Figure 5d. The reader is referred to the literature references for a detailed discussion of the mathematical and theoretical treatments associated with these spectroscopic techniques.

## II. DIRECT CPMAS MEASUREMENTS OF WHOLE SOILS

The first solid-state  $^{13}\text{C}$  NMR spectra of whole soil were reported in 1981 by Barron and Wilson.<sup>26</sup> Ideally, the tool or technique employed in the analysis of soil organic matter should be nondestructive. Until the advent of CPMAS, structural group analysis, characterization of soil humic and fulvic substances, and other soil components could not be performed adequately without chemical alteration during pyrolysis and extraction procedures. Therefore, a degree of doubt existed as to how representative the measurements were in terms of the actual soil, *in situ* structure and composition. Particularly, a controversy exists even now regarding the aromaticity of soil organic matter.<sup>26-28</sup> A number of reasons for such controversy will be discussed below. Additionally, precautions will be stated which should be adhered to in order to prevent similar mistakes based upon "ideal?" methods, such as CPMAS.

Preston and Ripmeester published the spectra of several whole soils and some of their fractions as shown in Figure 8.<sup>29</sup> The  $^{13}\text{C}$ -CPMAS spectra of the various organic soils show some common features. Resonance peaks were identified at 30 ppm and assigned to unresolved methyl, methylene, and methine carbon nuclei. Methoxyl carbon is seen at approximately 58 ppm. Carbon attributed to carbohydrate is indicated by resonances around 74 ppm (carbohydrate ring structures) and at 104 ppm (the anomeric region). Further assignments include the region from 50 to 70 ppm where N-substituted carbon, possibly from amino acid residues, gives a small

**Table 2**  
**SOLUTION-STATE VS. HIGH RESOLUTION SOLID-STATE NMR**  
**SPECTROSCOPY**

Total interaction	=	Zeeman	+	Dipolar	+	Scalar	+	Chemical shift
Solution state		50 MHz		0		200 Hz		Isotropic, single frequency
Solid state		50 MHz		50 kHz		200 Hz		200 ppm-wide chemical shift anisotropy
Solid state NMR technique used to overcome broadening				High-power (dipolar) proton decoupling		High-power decoupling also removes J-coupling		Magic-angle spinning gives the isotropic line

*Note:* This is a specific example showing  $^{13}\text{C}$  nuclear spin interactions in a 4.7-T field.

From Jelinski, L. W., *Chemtech*, March, 1986, 188. With permission.

contribution.<sup>30</sup> Somewhat lower levels of intensity are evident in the aromatic region ranging from about 110 to 160 ppm. Resonances can be assigned at approximately 130 (C- and H-substituted C) and at 150 ppm (O- and N- substituted C). The peak at 174 is indicative of carbonyl type carbon and may be assigned to carboxyl, amide, and ester group linkages. The results of various groups indicate that studies of soil organic matter are being performed and may be potentially correlated to variations in soil formation, function, and vegetation coverages. Further information is available in the references already cited as well as the others which are listed.<sup>31,32</sup>

## A. Experimental Conditions — Spin Dynamic Considerations

### 1. NMR Spectrometer Settings

To obtain reasonable information on such complex materials, certain experimental and instrumental parameters must be considered. Current high-field, high-resolution NMR instruments are stable in terms of the  $B_0$  field and also with regard to magic angle settability and spinning speeds. Problems are encountered however, in initially getting samples to spin at 4 to 6 kHz, but these are generally not insurmountable. Samples suitable for analysis are generally packed into rotors which are then spun by light gases in stators of various design. An excellent discussion of rotor and stator design has been given by Fyfe. He presents the advantages and disadvantages of such equipment as well as design and material modifications which have transpired since the original designs were reported.<sup>33</sup> Modern MAS devices are based upon the designs of Andrew and Lowe.<sup>20,34</sup> Their designs are depicted schematically in Figure 9.<sup>33</sup> Variable temperature MAS is also possible, and devices have been introduced for this purpose as well.<sup>35</sup> Upon completion of the experiment, the sample is returned to the scientist intact, unmodified, and preserved for further experimental study by other techniques.

### 2. Degree of Cross-Polarization Enhancement

During the CP process, a number of relaxation processes (mechanisms) must be considered in order to establish that spectral intensities are not distorted. Of the techniques described for obtaining CPMAS spectra, matching of the abundant  $^1\text{H}$  spin and the dilute  $^{13}\text{C}$  spin rotating frame Larmor frequencies to induce CP energy transfer is the most critical for controlling the relative magnetization or intensity response exhibited by the  $^{13}\text{C}$  resonances. Because the abundant protons in organic solids are close together, rapid spin diffusion occurs within this population. This process allows all protons within an individual component to have the same

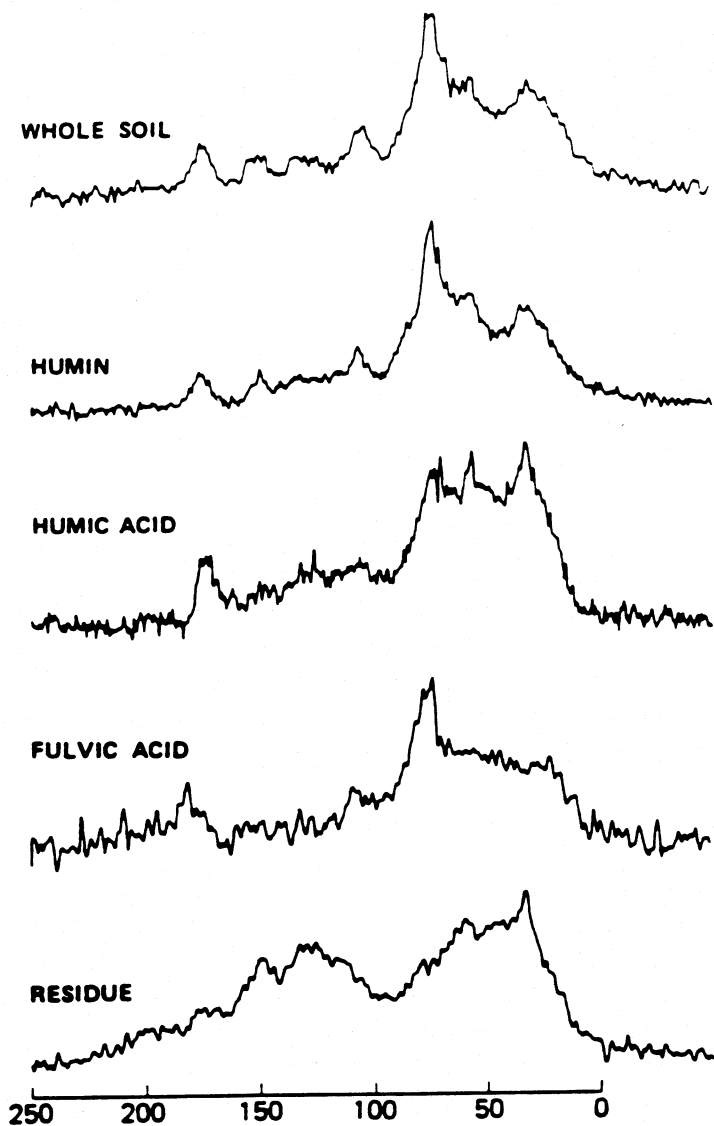


FIGURE 8. Solid-state CPMAS  $^{13}\text{C}$  spectra for organic soil A. humin, HA, fulvic acid, and residue of acid hydrolysis. (From Preston, C. M. and Ripmeester, J. A., *Can. J. Spectrosc.*, 27, 700, 1982.)

relaxation behavior. If spin diffusion is not uniform within a solid due to heterogeneity, the proton relaxation processes can differ for each component. Amorphous heterogeneous samples usually have  $T_{1H}$  values between 0.1 and 0.2 s as a result of local motions and amplitude variations. The first relaxation process which must be considered is called the contact time (CT). The CT is a period (millisecond range) when the proton and carbon spin reservoirs are in thermal contact with each other. The CP rate depends on the internuclear distance ( $r_{\text{CH}}^{-6}$ ) between carbon and hydrogen. Clearly, nonprotonated carbon nuclei will cross polarize at a slower rate than will protonated species.<sup>37,38</sup> The time constant associated with the carbon-proton CP process is referred to as the  $T_{\text{CH}}$ . In Figure 4, the buildup of  $^{13}\text{C}$  magnetization (dashed line) at the expense

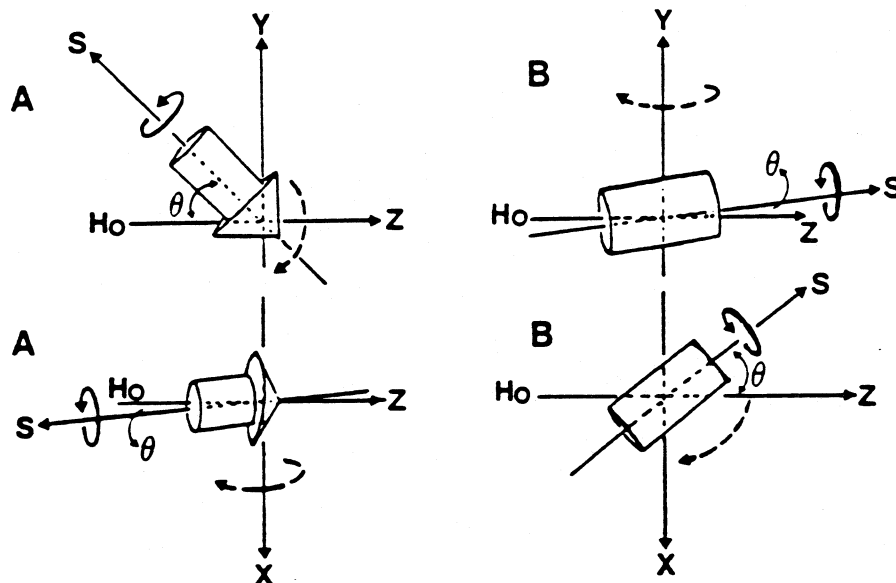


FIGURE 9. Schematic representation of the geometric arrangements for MAS using (A) the Andrew-Beams design and (B) the Lowe design. (From Fyfe, C. A., *Solid State NMR for Chemistry*, CFC Press, Guelph, Ontario, 1983, 272. With permission.)

of the  $^1\text{H}$  spin population is seen. However, a competitive relaxation is also occurring,  $T_{1\rho\text{H}}$ , known as the proton spin-lattice relaxation time in the rotating frame. This time constant reflects the decay or loss of proton polarization as a function of time. Typically,  $T_{\text{CH}}$  values are in the range of  $50\ \mu\text{s}$  to  $1\ \text{ms}$ . Because of this dependence on  $T_{\text{CH}}$  not all carbons are equivalent. Some carbons are isolated from neighboring protons (e.g., carbonyl carbons, tetra-substituted double bond carbons, and quaternary carbons) while others have directly bonded protons (e.g., methylene, methine, and methyl group carbons). For quantitative work, the observed carbon resonance intensities must be proportional to the number of carbons of any given type. This means that the carbons that cross-polarize slowly must be given adequate time to equilibrate with the spin-locked protons which are concurrently decaying during the time impacted upon by the  $T_{1\rho\text{H}}$  process. To satisfy this requirement, it is essential that the value of  $T_{1\rho\text{H}}$  be greater (order of magnitude) than the corresponding  $T_{\text{CH}}$  for each carbon population in the system. Figure 10 illustrates this point. In the early part of the contact period when the proton population has had minimal time to decay (proton population with a long  $T_{1\rho\text{H}}$ ), optimal energy exchange is achieved and a large  $^{13}\text{C}$  signal is generated. However, for those carbons having  $T_{\text{CH}}$  values closer to the proton  $T_{1\rho}$ , a significant amount of proton magnetization has been drained off before sufficient energy is interchanged. The result is a much diminished  $^{13}\text{C}$  signal, even when the experiment is optimized at a somewhat longer CT. Finally, when the protons have decayed to the point where there is little or no magnetization left ( $T_{\text{CH}} \gg T_{1\rho}$ ), virtually no  $^{13}\text{C}$  signal is observed. In general, this situation is not observed unless the carbons under consideration are significantly isolated from any protons, as has been found in some selected coal samples.<sup>17</sup>

Assuming the criteria of proton  $T_{1\rho} \gg T_{\text{CH}}$  is met, one must also consider the relationship between the experimental parameter, CT, and these decay times. In general, the CT should be much larger than the largest  $T_{\text{CH}}$  value in the sample (approximately a factor of five to ten), and much smaller than the proton  $T_{1\rho}$  (approximately one fifth the magnitude) to generate optimum responses.

In solid-state CP experiments, power levels are also very critical. Modulation of proton interactions (decoupling) in a solid requires approximately ten times more power than employed in solution state spectroscopy to achieve acceptable responses. Deviations in the power levels of the  $^1\text{H}$  or  $^{13}\text{C}$  transmitters can be very deleterious.  $T_{\text{CH}}$  values can be increased if the CP

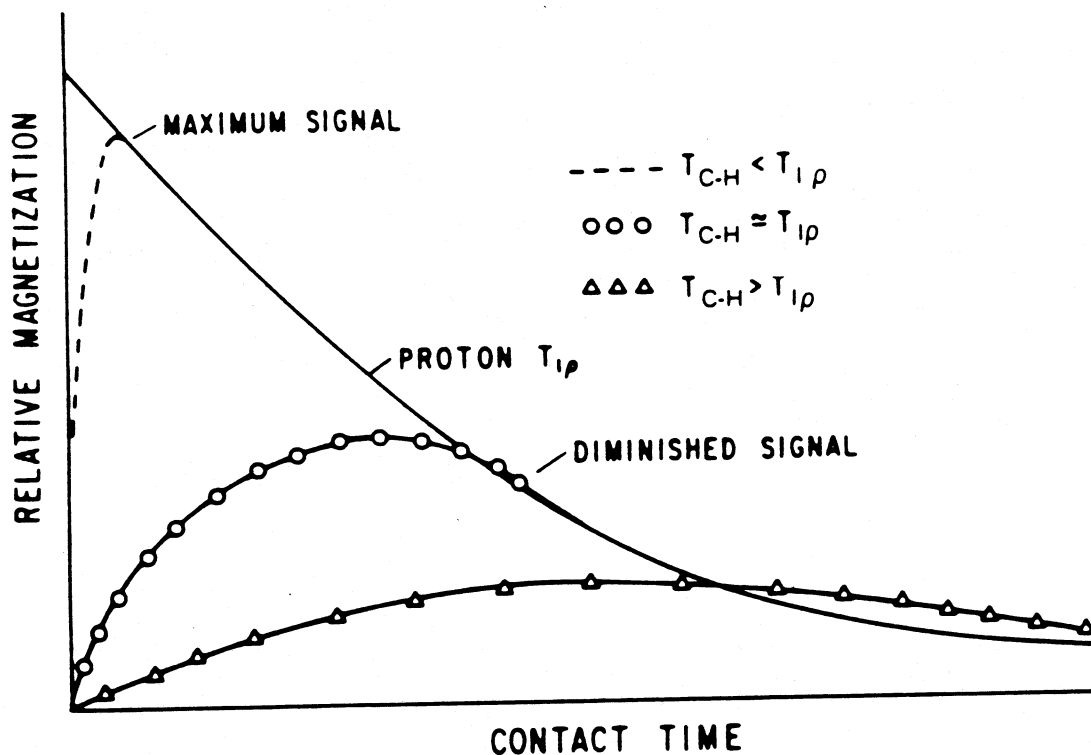


FIGURE 10. Competing relaxation processes during CP. (From Pfeffer, P. E., *J. Carbohydr. Chem.*, 3, 613, 1984. With permission.)

Hartmann-Hahn matching condition is not met. In the case of weak C-H and H-H dipolar coupling (e.g., in systems with rapid motional changes occurring in the solid), signal intensities can be changed markedly if the rf output power of the  $^1\text{H}$  or  $^{13}\text{C}$  transmitter changes by even  $\pm 0.1$  dB.<sup>36</sup> Such deviations would affect the resonance signal area. Quantitation would not be feasible through integration of such peaks.

### 3. Model Response System for Soils, Mucks, Sludges, and Humic and Fulvic Systems

The importance of these response factors for predominant carbon types present in soil and soil related systems has been illustrated.<sup>39</sup> To establish the relative response of various components in a heterogeneous matrix such as soil, we initially examined a model multicomponent mixture. We do not wish to imply that the components which make up the model mixture are the only components present in soils and/or sludges. These model constituents were selected to represent the predominant carbon types evident in the spectra of the materials selected for this study. Prior to making these measurements, the relaxation values (proton  $T_1$  and  $T_{1\rho}$ ) of the individual compounds used to prepare the model system were evaluated (Figure 11 shows the  $^{13}\text{C}$ -CPMAS spectrum of each component used). The range of relaxation parameters was also measured in the presence of paramagnetic  $\text{Fe}^{+3}$  (in concentrations approximating sludge) to note its affect on each type of component. Organic free radicals and metal ions are present in soils and soil components. If these paramagnetic centers are removed, the structure of the sample will be modified. In solution, metal ions can exchange rapidly. In the solid however, different peaks may be broadened to different extents and even lost entirely from the spectrum. Note however, that in solution, cases of preferential metal ion complexation can cause different degrees of line broadening as well. Table 3 lists the proton  $T_1$  and  $T_{1\rho}$  values for the individual components in both the presence and absence of  $\text{Fe}^{+3}$ . All of these samples were prepared in a somewhat amorphous state by lyophilization from water. The final state of the lipid fatty acid component

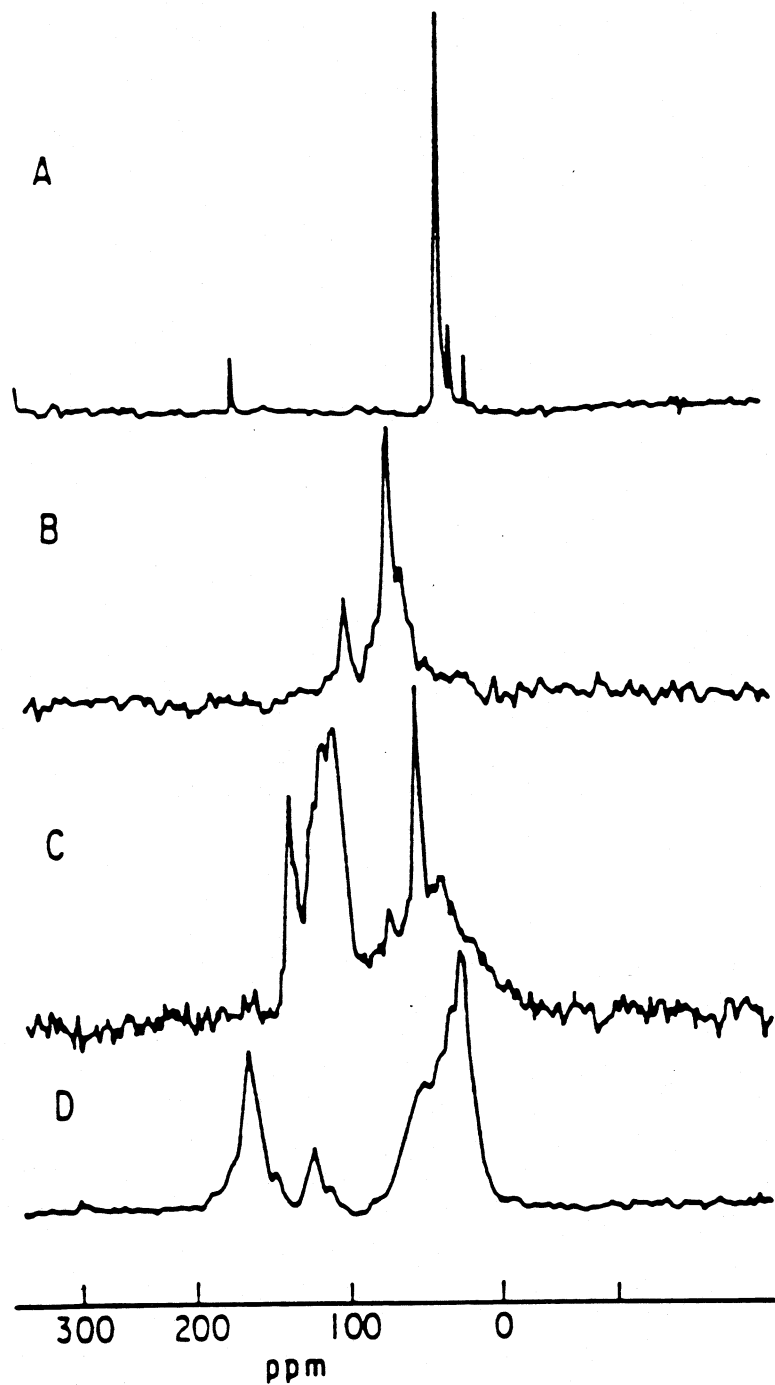


FIGURE 11. CPMAS  $^{13}\text{C}$  NMR spectra of reference compounds: (A) stearic acid, (B) wood pulp, (C) lignin, and (D) keratin. Each spectrum was obtained from 3000 acquisitions with a pulse delay of 1.5 s and a CT of 0.5 ms and 10- to 15-Hz line broadening. (From Pfeffer, P. E., Gerasimowicz, W. V., and Piotrowski, E. G., *Anal. Chem.*, 56, 734, 1984. With permission.)

in the model mixture appears to be somewhat more ordered than that of the other model compounds as evidenced by its extremely long  $T_1$  and  $T_{1\rho}$  values. The  $T_1$  and  $T_{1\rho}$  values associated with this hydrophobic component exhibit little change when the paramagnetic-amended system is compared to the analogous non-iron-containing mixture. Similarly, the hydrophobic nature of lignin does not foster intimate spatial communication with the  $\text{Fe}^{+3}$  since its  $T_1$  has only diminished by half while its  $T_{1\rho}$  has essentially remained the same. The more

**Table 3**  
**RELAXATION VALUES<sup>a</sup> OF MODEL COMPONENTS**

Component	Fe <sup>3+</sup> - <sup>b</sup>		Without Fe <sup>3+</sup>	
	T <sub>1H</sub>	T <sub>1pH</sub>	T <sub>1H</sub>	T <sub>1pH</sub>
Wood pulp	3.0	2.2	78.8	7.0
Lipids	2.5 × 10 <sup>3</sup>	18.6	5.0 × 10 <sup>3</sup>	21.0
Protein	9.1	3.8	83.0	4.7
Lignin	73.0	7.3	164.0	7.0
Microcrystalline cellulose	2.0	7.3	505.0	

<sup>a</sup> Milliseconds ± 10%.

<sup>b</sup> 1.9%.

From Gerasimowicz, W. V., Hicks, K. B., and Pfeffer, P. E., *Macromolecules*, 17, 2597, 1984. With permission.

hydrophilic carbohydrate and protein constituents of the model do, however, show signs of significant interaction with the paramagnetic centers. Iron-induced shortening of T<sub>1</sub> is evident in both the protein and carbohydrate. Researchers have exploited this concept through the addition of small quantities of paramagnetic species to pure peptides thereby reducing their proton T<sub>1</sub>s and recycling times while simultaneously enhancing the efficiency of the CPMAS experiment.<sup>40,41</sup> Such preferential shortening of T<sub>1</sub> can have a pronounced effect on <sup>13</sup>C sensitivity when one uses a recycling time of 4 to 5 T<sub>1</sub>s. In our sample, the large spread of proton T<sub>1</sub> values necessitates the use of pulse delay values of 20 and 10 s, respectively, in the absence and presence of 1.9% Fe<sup>3+</sup> to ensure reestablishment of nearly total proton equilibrium magnetization.

The rate of proton relaxation, T<sub>1p</sub>, presents a different problem when trying to establish equal carbon population responses. A CT must be selected which will be fast enough to facilitate carbon-proton energy transfer for the components with rapidly relaxing protons (short T<sub>1p</sub>s) as well as those with long T<sub>1p</sub> values.<sup>42,43</sup> This question has been addressed in a paper concerning the analytical reliability of the solid-state <sup>13</sup>C spectra of coals.<sup>42</sup> Yoshida et al. examined the effect of pulse repetition rates and CTs on the <sup>13</sup>C solid-state spectra of a coal sample and a hexane-soluble fraction.<sup>44</sup> Optimal CTs and pulse delays were required to obtain reliable estimates of carbon aromaticity in their sample.<sup>45</sup> Unlike the heterogeneous models and sludges examined in this work, the coal samples contained compounds of limited diversity, e.g., aliphatic and aromatic hydrocarbons, with a relatively narrow range of T<sub>1p</sub> values. As seen in Table 3, the dynamic range of T<sub>1p</sub> values in the present study is exceedingly large even for the metal-free components (~7.0 ms to 21.0 ms). In order to maximize the absolute <sup>13</sup>C responses of the model mixture, a study of the contact time vs. intensity of our model mixture in the presence and absence of Fe<sup>3+</sup> as found in sludge mixtures was performed. In these systems, with and without Fe<sup>3+</sup>, the rapid growth of the carbohydrate resonances at ~70 ppm and 102 ppm as well as the aliphatic resonances at ~30 ppm in the range of CTs 0.03 ms to 0.5 ms was observed. From 0.5 ms to 7.0 ms there is a rapid loss of signal from the carbohydrate peaks while the aliphatic peak, having long T<sub>1p</sub> values (21.0 ms no Fe<sup>3+</sup>, 18.6 ms Fe<sup>3+</sup>), clearly persists. Cross-relaxation effects on the protein and lignin resonances are more difficult to assess because of their overlap with each other and with the aliphatic region. For both the metal- and nonmetal-containing samples, the maximum response for both components (lipid and carbohydrate) is found at a contact time of about 0.5 ms. Figure 12 illustrates the generation of carbon magnetization for the Fe<sup>3+</sup>-containing model system as a function of variable CT. At the shorter contact times (<0.5 ms) necessary to overcome the rapid proton relaxation process, the relationship of T<sub>CH</sub> << CT

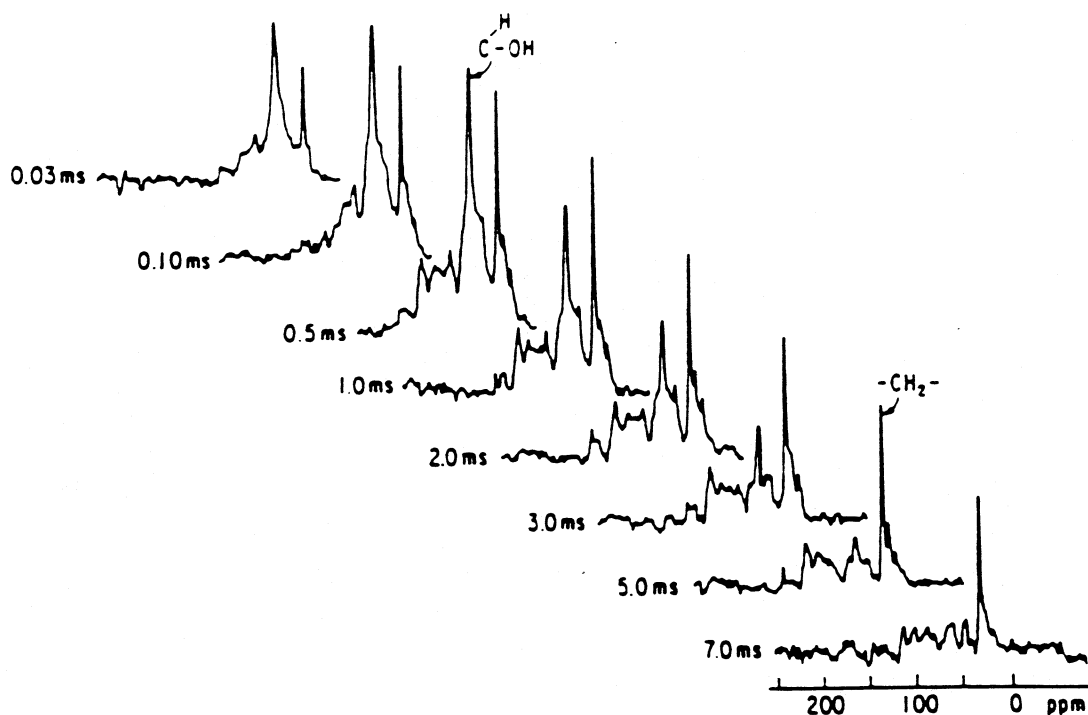


FIGURE 12. CT study of model sludge mixture containing 1.9%  $\text{Fe}^{3+}$ . Each spectrum was obtained after 5000 scans, a pulse delay of 1.5 s, CTs of 0.03 to 7.0 ms, and 15-Hz line broadening. (From Pfeffer, P. E., Gerasimowicz, W. V., and Piotrowski, E. G., *Anal. Chem.*, 56, 734, 1984. With permission.)

becomes invalid and loss of absolute  $^{13}\text{C}$  intensity is apparent. This phenomenon is clearly illustrated when the spectra of the model mixture is examined under optimum conditions with and without metal as seen in Figure 13. In spectrum 13A we see that the ratio of the carbohydrate resonances at  $\sim 102$  ppm and  $\sim 70$  ppm (corrected for lignin content) to the aliphatic region at  $\sim 30$  ppm is  $(2.2/1.0) \pm 10\%$  (theory 2.1/1). Spectrum 13B, in the presence of 1.9%  $\text{Fe}^{3+}$  with the aliphatic region normalized to the aliphatic region of 13A, shows a ratio of carbohydrate/lipid of only  $(1.1/1.0) \pm 10\%$ . From these data it is obvious that even under these most optimum conditions of short CTs of 0.5 ms and long recycling times of 20 s, 48% of the carbohydrate signal has been lost. At these high  $\text{Fe}^{3+}$  concentrations (1.9%), preferential loss of proton polarization associated with the carbohydrate species is observed. The  $\text{Fe}^{3+}$  concentration dependence of the phenomenon can be seen in Table 3.

The lost  $^{13}\text{C}$  intensity is due to the loss of magnetization for those carbons that have severely diminished  $T_{1\rho}$  values relative to their corresponding cross-relaxation times ( $T_{\text{CH}}$ s). While  $^1\text{H}$  spin polarization is being transferred to all of the components in the model, the short proton  $T_{1\rho}$  associated with the carbohydrate component upon paramagnetic doping causes a loss in its signal intensity much more rapidly than any decay seen in the other constituents with their longer  $T_{1\rho}$ s. The regime of  $T_{\text{CH}} \ll \text{CT} \ll T_{1\rho\text{H}}$  is difficult to meet in our model system for the carbohydrate component in the presence of large quantities of paramagnetic iron. This effect is reflected in the wide dynamic range of proton  $T_{1\rho}$  values seen in Table 3. If one cannot account for all carbon in a sample in an absolute sense, the fraction of carbon resonances must at least be representative of all carbon in the sample. The preferential localization of Cu in the carbohydrate or hydrophobic portions of soil organic matter has been reported. However, the effects are less dramatic than those shown here. These authors further concluded that carbohydrates such as uronic acids may account for the metal-binding effects. The importance of such soil components and their ability to bind metals is well established.<sup>47,48</sup>

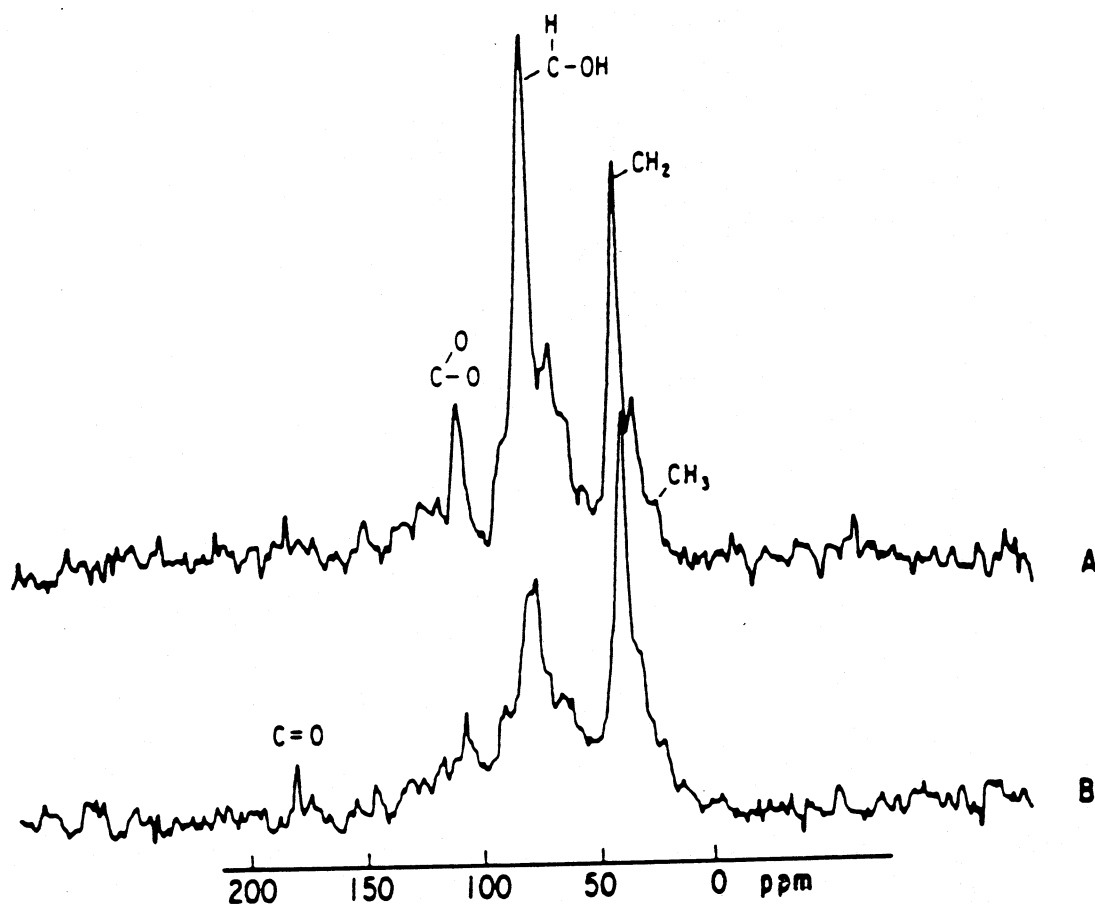


FIGURE 13. Comparison of  $^{13}\text{C}$ -CPMAS NMR spectra of model sludge mixtures (A) with no  $\text{Fe}^{3+}$  and (B) containing 1.9%  $\text{Fe}^{3+}$ . Each spectrum was obtained under optimized conditions. 14,000 scans, 16-s pulse delays, a 0.5-ms contact time, and 20-Hz line broadening. (From Pfeffer, P. E., Gerasimowicz, W. V., and Piotrowski, E. G., *Anal. Chem.*, 56, 734, 1984. With permission.)

#### 4. Humic Substances

Several recent reviews are available on solid-state NMR and humic matter.<sup>49-53</sup> Our purpose is not to provide another review but rather to cite some further examples and techniques which will be useful to the soil scientist in applications to agricultural systems, and to stimulate further developments in these areas. Humic materials are known to be involved in a number of interrelated, chemical processes in soil, and to influence plant growth directly as well as indirectly. Indirectly, humic acids (HAs) may improve soil fertility by increasing the availability of plant nutrients or by sequestering toxic heavy metals in the soil environment. Kononova suggested early on (1966) that plant roots can assimilate these naturally occurring heteropolymers thereby directly affecting plant growth and metabolism.<sup>54</sup>

Humic substances derived from terrestrial plants differ in chemical structure from those originating from aquatic plants.<sup>55-58</sup> One extraction scheme is depicted in Figure 14.<sup>59,60</sup> Figure 15 shows some representative spectra of HAs.<sup>50</sup> Signals are evident from 110 to 160 ppm (aromatic/olefinic and carboxyl groups are seen from 160 to 190 ppm. Paraffinic and carbohydrate signals constitute the largest area in Figure 15. Carbohydrates originate from the fact that at this soil horizon nondegraded plant litter is present. Therefore, during the treatment with base, hemicelluloses and other carbohydrates are being extracted. Hatcher comments further on the notion that large amounts of paraffinic carbon in HAs may affect the determination of aromaticity for these substances.<sup>50</sup> The relative intensities of the paraffinic resonance ranges from 7.1 to 36% in this case. Aromaticities determined from chemical degradation methods can range from 61 to 100% and are generally higher than those ascertained from NMR methods.<sup>61</sup>

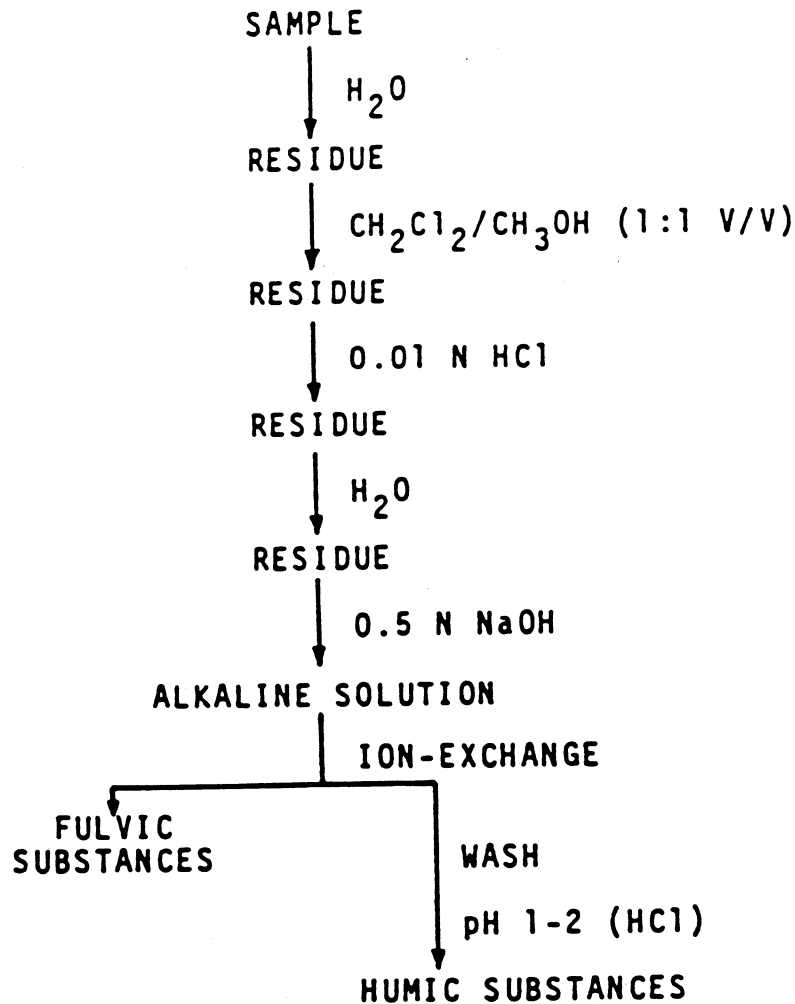


FIGURE 14. Humic substance extraction scheme (all extractions were performed in an  $N_2$  atmosphere). (From Gerasimowicz, W. V. and Byler, D. M., *Soil Sci.*, 139, 270, 1985. With permission.)

Controversy, however, does exist as to the accuracy and detection of all components based upon the considerations mentioned above, and it is still not clear as to which of the methods (traditional or solid-state NMR) is the more accurate. The problem of detection is discussed at length below.

In order to establish stable cropping systems, soil fertility and structure must be maintained. Soil organic matter is vital to this stability in that the organic matter serves as a source of nutrient elements which can be released through mineralization. Cultivation of a soil previously supporting pasture or native vegetation generally leads to reduced levels of soil organic matter.<sup>62,63</sup> Decreases in organic carbon from five Vertisol soils ranged from 31 to 59% after 25 years of continuous cultivation for cereal crops in southern Queensland.<sup>62,63</sup>

Skjemstad et al. studied a soil type which had been under cultivation for as long as 45 years.<sup>64</sup> These soils were Langlands-Logie clays used primarily for wheat production in Queensland. Samples were collected from fields (and fractionated as described in the reference) which varied in their time of continuous cultivation from 20, 35, and 45 years.<sup>64</sup> A sample was also examined from an adjacent area which had never been cultivated and which was under virgin brigalow (*Acacia harpophylla*) scrub. Over the same time course as the cultivation process, organic matter levels dropped by 50, 61, and 66% (as determined by chemical analysis).<sup>64</sup> However,  $^{13}C$ -CPMAS spectroscopy performed directly on these samples, and on the uncultivated virgin soil, does not reveal significant differences in the *in situ* organic.

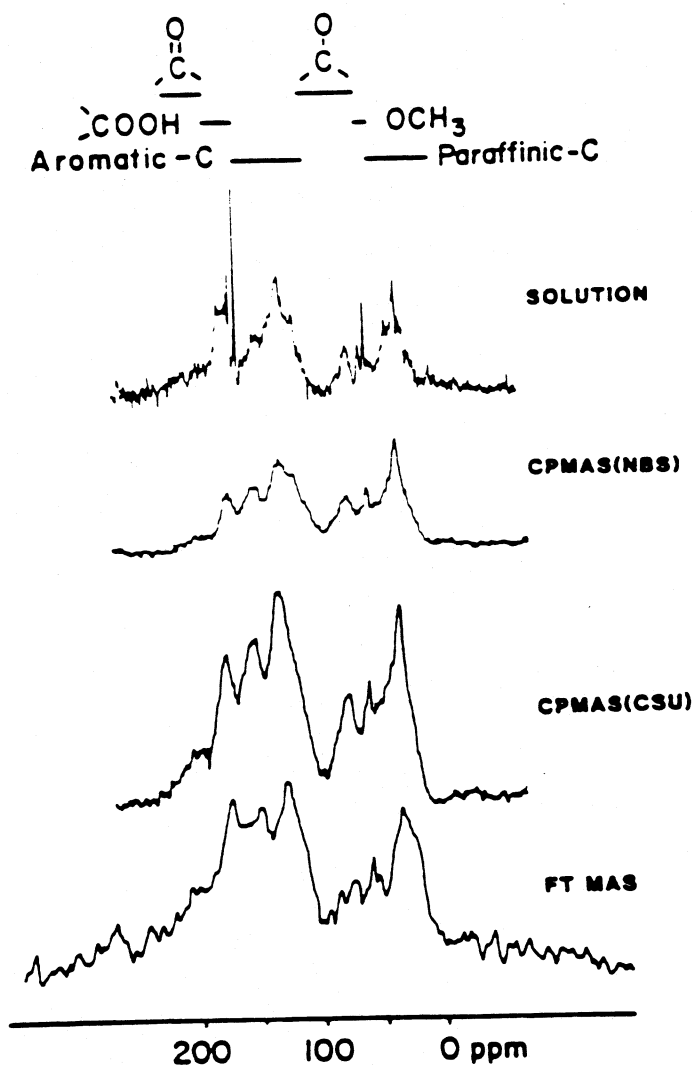


FIGURE 15.  $^{13}\text{C}$ -NMR spectra of humic acids from the Rice Lake peat sample obtained in solution (0.5 N NaOD) and in solid state by CPMAS and by conventional Fourier transform (FT) with MAS. (From Hatcher, P. G., Berger, I. A., Dennis, L. W., and Maciel, G. E., *Aquatic and Terrestrial Humic Materials*, Christman, R. F. and Gjessing, E. T., Eds., Ann Arbor Science, Ann Arbor, MI, 1983, 37. With permission.)

Such discrepancies may be attributed to lack of CP as well as paramagnetics which may, for example, affect the ratio of aromatic/carbonyl functional groups. Furthermore, the HA fractions were shown to decrease as a function of cultivation time, while the relative concentration of clay-associated matter increased. The authors state that UV-visible and IR analysis agreed with the NMR. The investigators concluded that the most resistant, and therefore stable, organic components are those physically associated with the inorganic components of the soil. As such, these materials were inaccessible to enzymatic or chemical substances, rendering them inert to degradation. In a  $^{13}\text{C}$ -NMR solution study, Cartoux and Schnitzer reported the characteristics of the organic matter in particle size fractions separated from an Aquoll.<sup>65</sup> The samples were from the surface horizon of the cultivated Aquoll. HAs and residual humic substances (obtained from the residue of the HAs by treatments with HCl-HF and reextracting) were analyzed. The chemical analyses showed that the five silt fractions had the highest carbon and nitrogen concentrations. The  $^{13}\text{C}$ -NMR spectra showed that the HAs derived from the clays were richer in aliphatics than HAs derived from larger classes of particles. The residual HAs were more homogeneous in

**Table 4**  
**DETAILS OF SAMPLES USED**

Sample	Parent material
Ornithogenic soil	Guano deposits collected from several locations in Antarctica (i.e., Cape Adare, Cape Hallet, Cape Bird, Cape Crozier, and Inexpressible Island)
Antarctic moss	Under dead mosses consisting of comminuted (whole) and visible organic matter of <i>Bryum antarcticum</i> and <i>Bryum argenticum</i> mosses
Antarctic peat	Polytrichum moss from Signy Island, British Antarctic Peninsula

From Wilson, M. A., Goh, K. M., Collin, P. J., and Greenfield, L. G., *Org. Geochem.* With permission.

composition than the HAs. Thus, their structures are more stable than the HAs. So, these data also appear to be consistent with the idea that the organic matter associated with inorganic soil components is more resistant to environmental decomposition than the unassociated fraction.

In all of the studies cited, the reader should bear in mind that the results apply only to the systems under investigation. One should not necessarily attempt to apply interpretations or trends observed in one system to another system.

Clearly, NMR analysis has demonstrated the variability in the structure of organic matter in soils and extracts from the soils. The fraction of aromatic carbon to total carbon has been a particularly sticky problem, where values ranging from 10 to 74% have been reported.<sup>58,61,66</sup> Similarly, large variations in carbohydrate content have been reported.<sup>31,58,61</sup> Specific reasons for such differences have not been clearly elucidated. Furthermore, little information is available as to the reason(s) for relatively high carbohydrate content in soils. Thus, Wilson examined humic substances from the Antarctic continent (terrestrial HAs) where lignin is a negligible portion of the vegetation.<sup>67</sup> The soil humification rate should be very slow compared to warmer climates, thus preserving organic matter in its native state.

The samples obtained are described in Table 4.<sup>67</sup> Solid-state <sup>13</sup>C-CPMAS spectra are shown in Figure 16.<sup>67</sup> The Antarctic peat sample appears to be composed predominately of carbohydrate. Resonances are seen at 99.8 ppm from C-1 dioxygenated carbons and at 78.8 and 63 ppm from hydroxylated carbons. The HA fraction also shows carbohydrate at 71 ppm. The overall spectrum of the HA is more complex than that of the peat sample. Resonances at 56 ppm may be assigned to methoxyl carbons or even amino carbons. With dipolar dephasing (see discussion below), the 56 ppm resonance persists, therefore it arises from methoxy as opposed to amino-like moieties.

The spectrum of the fulvic acid fraction from the moss sample (not shown) suggests that the fulvic acid consists of two carbohydrates.<sup>67</sup> The authors assign these carbohydrates to a mixture of  $\alpha$  and  $\beta$  glucose units. The fulvic acid fraction appears to be derived from hydrolysis of cellulosic components.

Furthermore, the spectra shown indicate that while aromatic components are evident in soils without appreciable lignin, lignin is not necessarily the precursor for the aromatics. Thus, other factors, such as microbial activity, may contribute and alter aromaticity. Temperature changes have an important environmental impact on humus formation, and when organic turnover rates are slowed down, carbohydrate content is high when compared to soil systems from warmer environments.

Soil humic materials are thought to be a source for some of the dissolved organic carbon (DOC) found in natural waters. Many components and compound types have been identified, such as amino acids, carbohydrates, and fatty acids.<sup>68</sup> The difficulties associated with understanding the chemistry of terrestrial humates are compounded in the case of freshwater and marine environments due to the problem of isolating sufficient quantities of organic matter from such sources. Yet, marine environments are the second largest reserve of organic carbon on this

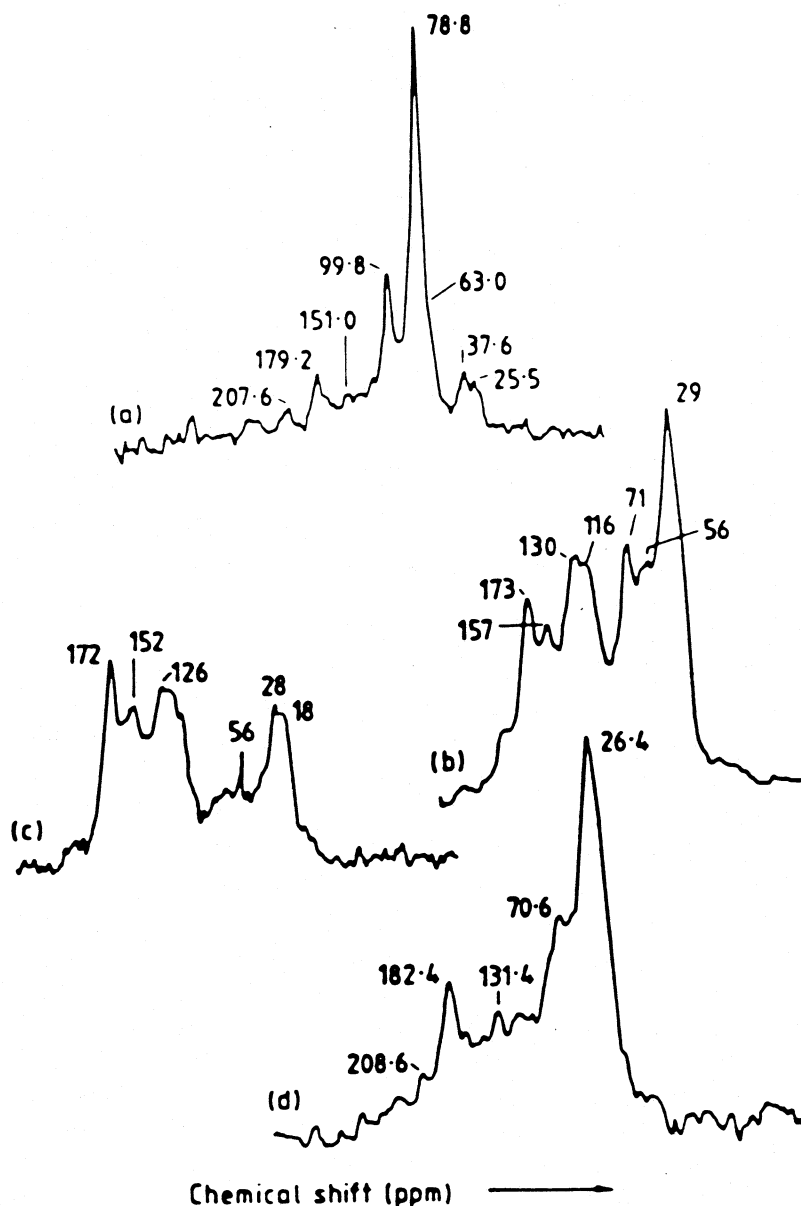


FIGURE 16.  $^{13}\text{C}$  CPMAS spectra of (a) Antarctic peat, (b) HA from Antarctic peat, (c) 40- $\mu\text{sec}$  dipolar dephased spectrum of HA from Antarctic peat, and (d) HA from soil under moss. (From Wilson, M. A., Goh, K. M., Collin, P. J., and Greenfield, L. G., *Org. Geochem.*, 9, 225, 1986. With permission.)

planet, (sediments contain the largest reserves) with an estimated  $800 \times 10^9$  tons, 89% of which is dissolved.<sup>69</sup> Some of the factors which influence humate chemistry and structure are shown in Table 5.<sup>70</sup> Geography, environment, vegetation, and microbial activity all act synergistically to affect soils and humic substances. Transport of humic substances which are water soluble can also affect the composition or mixture found at any particular site or location.

A study has been reported which attempted to link the relationship of dissolved marine humics with phytoplankton.<sup>71</sup> The reader is referred to the reference for a detailed discussion of the isolation procedures.  $^{13}\text{C}$ -CPMAS spectra are shown in Figure 17. The usual  $^{13}\text{C}$  resonance assignments can be made

1. 0 to 60 ppm, aliphatic carbon

**Table 5**  
**FACTORS INFLUENCING THE STRUCTURE OF HUMIC SUBSTANCES**

Primary factor	Secondary factor	Influence
Geographical location/climate	Type of plant life	Produces variations in proportions of groups of chemical compounds, e.g., lignins Transformation (biodegradation/polymerization) or organic materials Structure of aquatic humic substances may reflect terrestrial input
	Microbial activity	
	Transport of humic substances	

From Gillman, A. H. and Wilson, M. A., *Org. Geochem.*, 8, 15, 1985. With permission.

2. 60 to 95 ppm, carbon singly-substituted with electron withdrawing elements such as oxygen or nitrogen in the case of humic substances
3. 95 to 110 ppm, dioxygenated carbon
4. 110 to 160 ppm, aromatic and olefinic carbon
5. 160 to 190 ppm, ester, amide, carbonyl, and salts thereof

Further analytical information is shown in Table 6 for the HA as well as for intra- and extracellular material and exudates of *P. tricornutum*. The marine humic material contains a large proportion of highly branched alkyl chains, and a smaller amount of aromatic. The authors also point out the presence of appreciable carbohydrate (uronic acid(s)). GC-MS analysis of the *P. tricornutum* exudates allows identification of furans (from carbohydrates), pyrroles, nitrites, phenols, and methylphenols.<sup>71</sup> Therefore, one can see the similarities between the exudates and the dissolved marine humic substances.

Dissolved organic matter (DOM) in pore waters from sediments of different depositional environments has also been examined by <sup>13</sup>C-CPMAS.<sup>72</sup> The DOM appears to exist mostly as two major types: one type is largely composed of carbohydrates and paraffinic functionality, whereas the second type is dominated by paraffinic and aromatic groups.<sup>72</sup> The authors conclude that the dominance of one DOM structural type over the other is dependent upon the oxidizing and/or reducing capacity of the sediment from which the materials are derived. Under one set of conditions (anaerobic) microbes can degrade carbohydrates and accumulate in the pore waters. Aerobic conditions show reduced carbohydrate and enhanced aromaticity, probably from lignin components.<sup>72</sup>

In the case of one particular aquatic humic substance, aromatic ketone groups were found to comprise the major portion of the carbonyl functionality.<sup>73</sup> Spectra of underivatized HAs and fulvic acids were compared and contrasted with chemically modified derivatives. The authors postulate that the mechanism of aromatic-ketone group formation could be attributed to photolytic rearrangement and oxidation of hydrocarbon and phenolic ester precursors.

The literature contains additional discrepancies in such measurements. For example, a recent comparison of solution and solid state spectra of HAs shows a nonconformity when functional group composition is determined for samples from Ap horizons of Typic Borolls near Indian Head, Saskatchewan.<sup>74</sup> These discrepancies were particularly emphasized in terms of the CO<sub>2</sub>H and phenolic regions.

Chemical degradation of four different humus types from Norway and analysis by <sup>13</sup>C-CPMAS NMR confirmed that 40 to 50% of the soil carbon is unaccounted for from among the degradation products.<sup>75</sup> More recently, spin counting experiments have been utilized in an attempt to account for the carbon in the HA and fulvic acid of geochemical samples, and the HA and fulvic acid fractions of soil organic matter.<sup>76,77</sup> The spin counting experiments involved obtaining spectra on mixtures of sample and glycine at varying contact times.<sup>76,77</sup> These spin

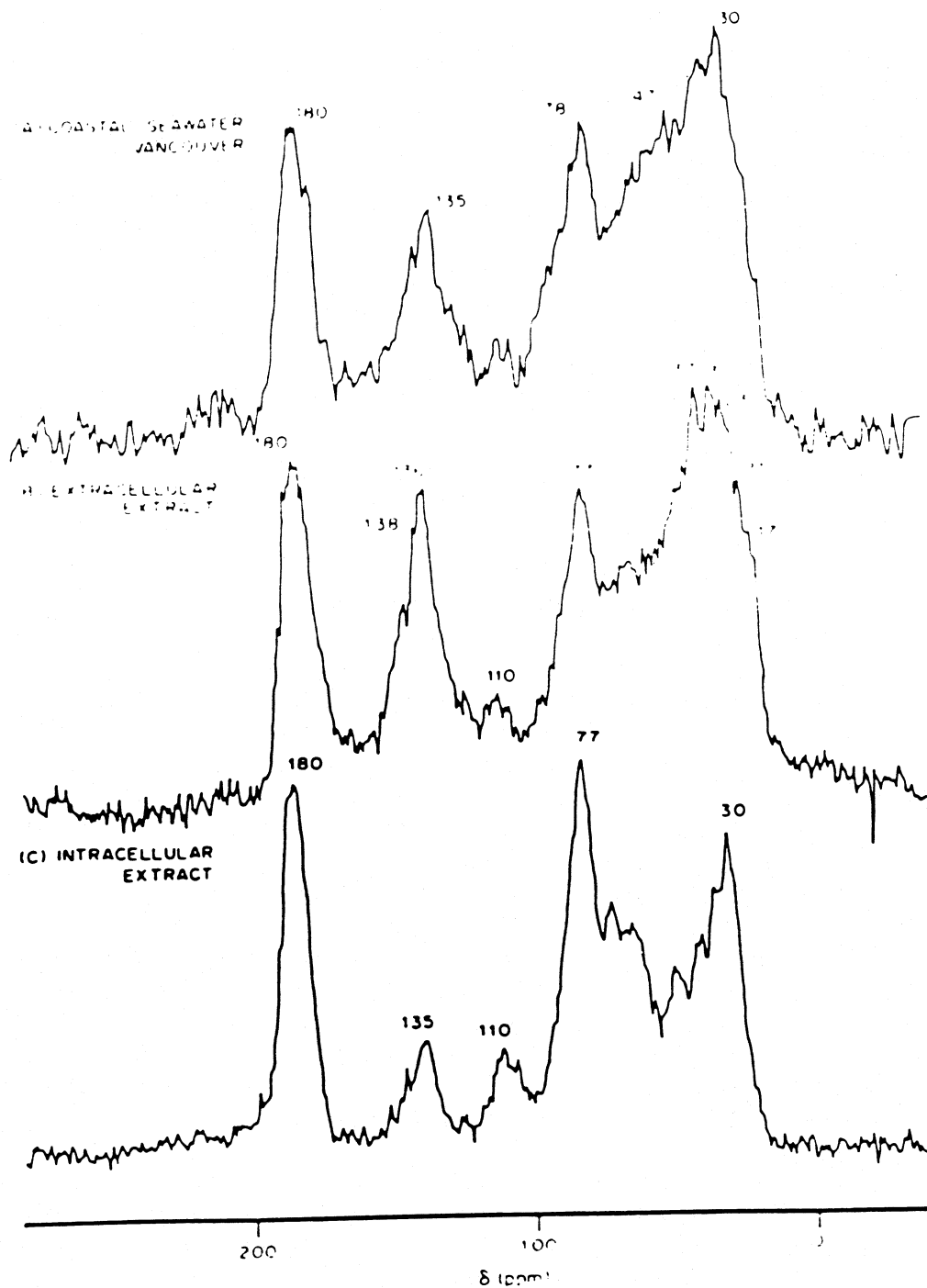


FIGURE 17.  $^{13}\text{C}$ -CPMAS spectra of humic materials. Resonances identified in Table 6. (From Gillman, A. H. and Wilson, M. A., *Org. Geochem.*, 8, 15, 1985. With permission.)

counting experiments demonstrated that less than 50% of the carbon from the various fractions examined was detectable in the NMR experiment. The differences were apparent even after correction for differential relaxation. Once again, the amount of aromatic and noncarbonyl aliphatic carbon was not in agreement with that determined by calculation methods.<sup>76,77</sup>

The question of aromaticity in soil humates has also been raised recently in a different light.<sup>78</sup>  $^{13}\text{C}$ -CPMAS studies were carried out on soil samples from the A horizons of a Typic Rendoll, Typic Xerorthent and two Typic Xerochrept(s) on different parent rocks (granite and shale, respectively).<sup>78</sup> The researchers found that the humic fractions were more aromatic than the

**Table 6**  
**RELATIVE AMOUNTS OF CARBON AND HYDROGEN TYPES IN HUMIC MATERIALS**

**Dissolved Seawater Humic Substances**

Sample	Method	% Hydrogen types				Method	% Carbon types				
		Aryl		O-Alkyl			Carboxyl <sup>c</sup>	Aryl <sup>d</sup>	Acetal	O-Alkyl	Alkyl
		H <sub>AR</sub> (6.1—9.0)	H <sub>R-0</sub> (3.0—4.7)	H <sup>a</sup> (1.8—3.0)	H <sup>b</sup> (0.5—1.8)						
Coastal sea water	— <sup>e</sup>	7	19	32	42	— <sup>f</sup>	14	18	2	18	49
<i>P. tricorutum</i> Extracellular material	— <sup>e</sup>	5	22	27	46	— <sup>f</sup>	15	19	3	15	49
<i>P. tricorutum</i> Intracellular material	— <sup>e</sup>	6	30	26	37	— <sup>f</sup>	21	6	7	42	25

<sup>a</sup> Largely hydrogen attached to carbon  $\alpha$  to aromatic rings or electron-withdrawing groups, such as carboxyl.

<sup>b</sup> Mainly alkyl protons  $\beta$  or further from aromatic rings or electron-withdrawing groups.

<sup>c</sup> Includes salt, ester, and amide groups.

<sup>d</sup> Includes olefinic carbon.

<sup>e</sup> By solution F.T. NMR.

<sup>f</sup> By CP/MAS-NMR.

From Gillman, A. H. and Wilson, M. A., *Org. Geochem.*, 8, 15, 1985. With permission.

humic fractions. The humic substances appear to have lower polysaccharide contents when the spectra are compared to those of the humins. The results were explained on the basis of the procedure employed in isolating the fulvic acids. The fulvic acids were isolated by using Polycar AT (a polyvinyl pyrrolidone polymer). Polycar AT preferentially retains polyphenols while partially excluding the polysaccharide fraction present in the extract at that point.<sup>78</sup> Fulvic acids isolated by means of adsorption onto charcoal exhibit higher polysaccharide concentrations than analogous Polycar AT preparations. Thus, the manner of isolation can impact on the final result observed spectroscopically.

Melanoidins have been synthesized from amino acids and sugars in various ratios and spectroscopically (<sup>13</sup>C-CPMAS) compared with humic substances from the Hula Basin in Israel.<sup>79</sup> The spectra showed significant similarities between the melanoidins and humics. The authors suggest that the Maillard reaction may be more important in the formation of humic materials than lignin-derived sources as traditionally assumed.<sup>79</sup>

One other important aspect of this report is the fact that aromaticities calculated from NMR data of the melanoidins are quite close to the aromaticities of both marine and terrestrial humic substances.<sup>79</sup> Thus, the issue of aromaticity persists.

Earl et al. have addressed relaxation processes which occur in fulvic acids and the effect of lowering the temperature in order to assure a quantitative response in CPMAS NMR spectra of this type.<sup>80</sup> Generally, researchers in this area have selected contact times of 1.0 to 2.0 ms with the belief that the correct relative intensities will be obtained even though the total response may not represent fully cross-polarized carbon. Such assumptions do not necessarily hold for heterogeneous mixtures such as fulvic acid. Other authors point out that CPMAS spectra of certain fulvic acids do not agree with their analogous high resolution solution spectra taken under quantitative conditions.<sup>81,82</sup> The most likely cause of such discrepancies was attributed to the CP and relaxation dynamics of the solid.

Figure 18 shows a series of <sup>13</sup>C spectra of Armadale fulvic acid taken under a number of conditions.<sup>80</sup> Spectrum A is the high-resolution solution data where the intensities are thought to be representative of the actual carbon content of the sample. Spectrum B illustrates the response upon Fourier transformation of simple Bloch decay data using MAS and high-power decoupling (no CP) at room temperature. Spinning sidebands are a cause of intensity distortion in this spectrum, making it relatively useless for quantitative evaluation. Figure 18C is a CPMAS spectrum (room temperature) of the sample. Intensity distortions are readily obvious due to varying relaxation domains as well as carbon-protein distortions in this material. Figure 18D depicts the spectrum under the same conditions as for C other than the temperature (lowered to -57 °C). Under such conditions several effects are assumed:

1. All extreme motions are frozen out
2.  $T_{CH} \ll T_{1\rho H}$
3. S/N is increased by a factor of three when compared to the room temperature data

The authors also point out that various chemical exchange reactions may be ongoing in these complex systems. Proton exchange could result in line broadening and unexpected chemical shifts. Line shapes are also a direct function of temperature.

These results strongly suggest that a combination of VT experiments, Bloch decay, and CT measurements are necessary to address the problems of molecular mobility and physical heterogeneity. A combination of such techniques is needed if one desires to advance beyond simple organic molecules in order to study complex natural products.

Clay minerals which are classified as smectites have the propensity to adsorb and take up small organic and polymeric species into their interlayers.<sup>81</sup> This intercalation or interlayer complex formation is generally seen to cause an increase in the basal spacing to distances of 10 Å or more. Through a combination of X-ray diffraction and <sup>13</sup>C-CPMAS along with chemical

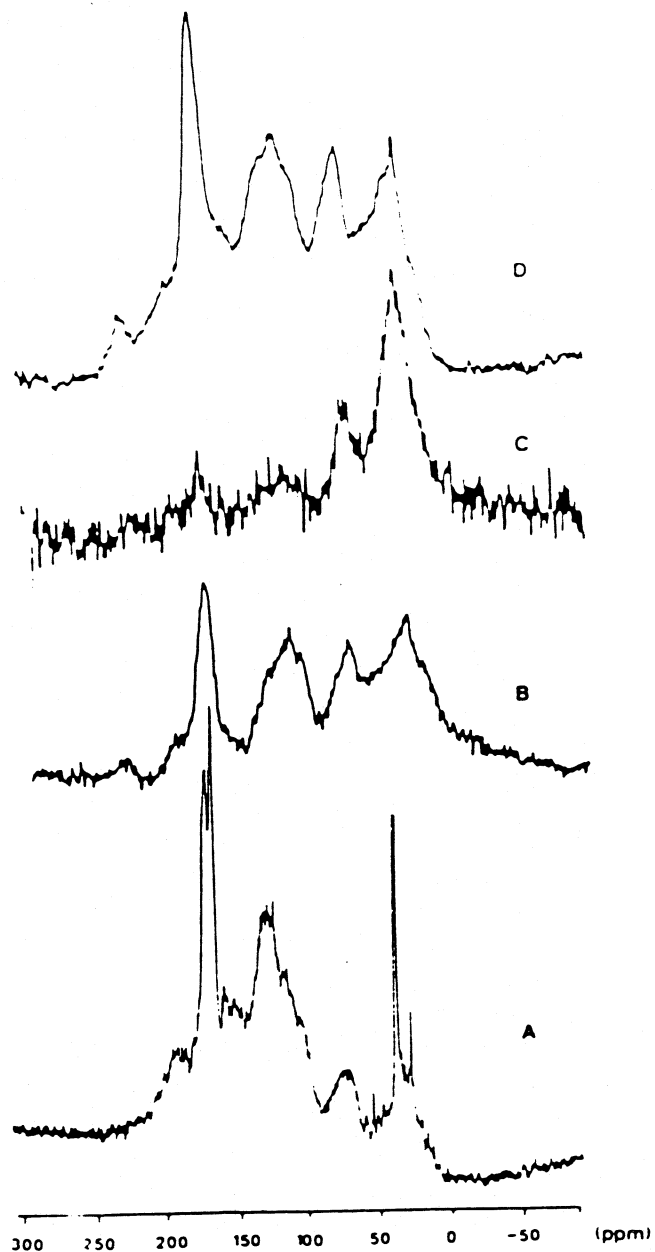


FIGURE 18. Four  $^{13}\text{C}$  spectra of the Armadale fulvic acid taken under different conditions. Spectrum A is the 75-MHz solution spectrum taken with 7500 scans using  $\pi/2$  pulse, a total interpulse delay of 10.2 s and inverse gated decoupling on a solution of 300 mg of sample dissolved in 2 ml of  $^{13}\text{C}$  depleted  $\text{DMSO-d}_6$  which is the sharp, truncated peak at 39.5 ppm. Spectrum B is the 50-MHz Fourier transform of a Bloch decay taken with 8192 scans at  $20^\circ\text{C}$  using a  $\pi/2$  pulse and a decoupling field strength of 60 kHz with MAS. Spectrum C is the 50-MHz CP spectrum at  $20^\circ\text{C}$  with 4096 scans and 0.5 ms CP CT. Spectrum D is the CP spectrum taken at  $-57^\circ\text{C}$  with 4568 scans and a contact time of 1.5 ms. (From Earl, W. L., Wershaw, R. L., and Thom, R. A., *J. Magn. Reson.*, 74, 264, 1987. With permission.)

and heat pretreatments, reasonable evidence has been presented for the occurrence of interlayer clay-organic complexes in several New Zealand soils.<sup>84</sup> The clay-mineral can be described as a mica-smectite. The organic species in question is characteristic of a humic substance with a

polymethylene chainlike structure.<sup>84</sup> The organic complex material was resistant to pyrophosphate extraction, decomposition, and peroxidation as seen in the NMR spectra. Furthermore, in the complex form, thermal stability up to 400°C was observed. Temperatures had to be raised above these levels in order to observe extensive decomposition.<sup>84</sup> Certain soil qualities were necessary in order to achieve such stability. These factors include a mineralogy of the clay smectite type, low microbial perturbation, and a highly acid soil environment.<sup>84</sup>

##### 5. Soil/Plant Components: Lignin-Carbohydrates — Interrupted Decoupling

Many terrestrial humic and soil components are aromatic. Much of this aromaticity is derived from vascular plant debris consisting of lignin and lignin analogue structures which impart the aromaticity to these systems. <sup>13</sup>C-<sup>1</sup>H interrupted decoupling and enzymatic degradation can be employed to infer details of structure in such constituents. A wood pulp sample (*Piceae glauca*) whose analytical characteristics have been previously described will be utilized to illustrate some of the salient features of interrupted decoupling.<sup>85</sup> The chemical composition of *Piceae glauca* pulp (PGP) consists predominantly of two major components; lignin and cellulose. Several <sup>13</sup>C-CPMAS NMR studies of lignin and cellulose in the solid state have been published.<sup>86-92</sup> These studies have focused on the assignment of resolvable resonances for these wood constituents. The assignments of the various peaks and signals from these reports on lignin, cellulose, and wood will be utilized in the interpretation of the <sup>13</sup>C-CPMAS spectra presented here. Although some of the referenced papers contain <sup>13</sup>C NMR solid-state spectra of lignin and cellulose from instruments operating at higher <sup>13</sup>C magnetic field strengths than that in our laboratories, the resolution obtained (upon careful examination of the published results) is not significantly enhanced over that observed here.

Figure 19A depicts the <sup>13</sup>C-CPMAS NMR spectrum of the PGP. Several resonance lines are clearly resolved in this spectrum. However, these bands are relatively broad and reflect the complex chemical composition of the sample, as well as its amorphous, noncrystalline structure. The rather broad resonance line widths also reflect the thermomechanical treatment, subsequent grinding, and preparation of the samples. Amorphous samples, such as those examined here, generally produce fairly wide NMR lines in solid-state <sup>13</sup>C-CPMAS spectra. The resonance at 105 ppm may be slightly narrower than similar resonances in ball-milled wood spectra.<sup>93</sup> This slight narrowing may reflect a small degree of crystallinity or nonamorphous regions in our samples. However, the extensive ball-milling as well as the spectral line widths observed essentially define the morphology of the PGP utilized in this work as amorphous. The spectrum shows that local molecular environments are nonequivalent within this polymeric network. The resolution achieved, however, is still adequate for identifying the major components of the PGP. The <sup>13</sup>C NMR spectrum is essentially dominated by resonances that are attributed to components arising from cellulose and hemicellulose. Carbon nuclei from these carbohydrate moieties give rise to signals between 60 and 110 ppm. The peak at approximately 105 ppm corresponds to the anomeric or C1 carbon from β-D-glucopyranose repeating units of cellulose. This resonance is particularly well resolved. The broad signals from the cellulose are superimposed on those from the hexose and pentose units of the hemicellulose compounds.

The spectrum also contains features which are less intense. The shoulder at 56.5 ppm may be assigned to methoxyl groups from lignin and also from hemicellulose. The aromatic components of lignin are seen between 130 and 155 ppm. These less intense features and the <sup>13</sup>C-CPMAS spectra cited and discussed so far only provide limited, qualitative information about the structure of these compounds. Other chemical and NMR methodologies are necessary to examine the chemical and structural relationship (connectivity) between lignin and carbohydrate in PGP and to enhance the underlying and unresolved components in the spectra obtained.

In order to enhance the spectral resolution of the noncarbohydrate components of the PGP, the <sup>13</sup>C-<sup>1</sup>H dipolar dephasing interaction was utilized.<sup>94</sup> Many examples now exist in the literature where dipolar dephasing provides spectra consisting only of resonances from

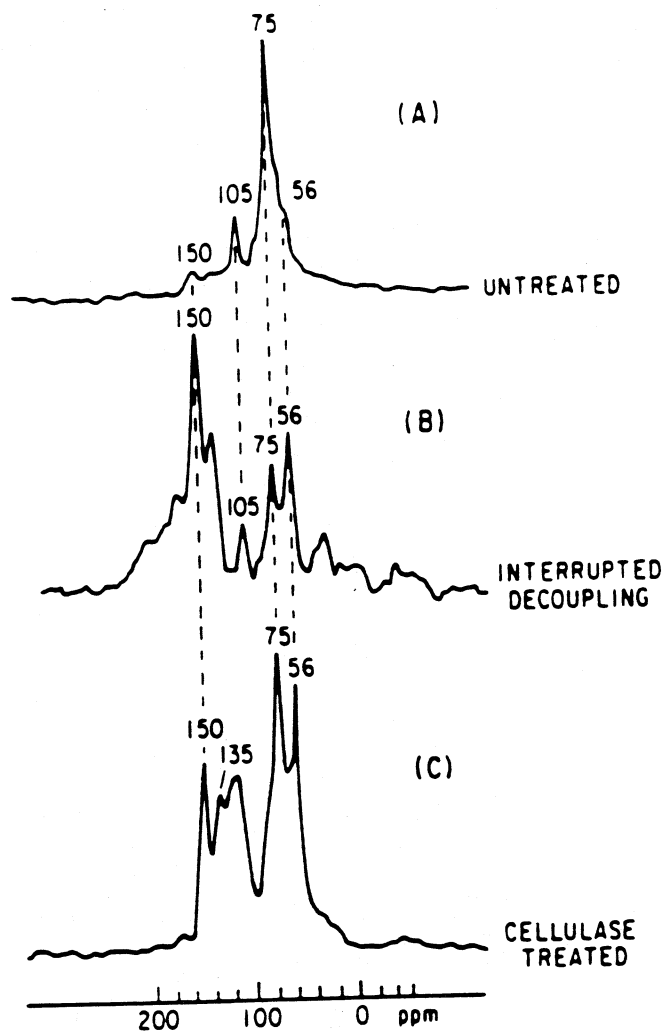


FIGURE 19. *Piceae glauca* pulp  $^{13}\text{C}$ -CPMAS spectra. (From Gerasimowicz, W. V., Hicks, K. B., and Pfeffer, P. E., *Macromolecules*, 17, 2597, 1984. With permission.)

nonprotonated carbon nuclei and methyl groups.<sup>94-98</sup> Certain functional groups, such as methyl groups, undergo rapid, internal rotations, even in the solid state. Such motion attenuates the  $^{13}\text{C}$ - $^1\text{H}$  dipolar relaxation mechanism rather markedly, with the result that resonances from such carbon nuclei are attenuated but not entirely eliminated from the spectrum. Even though the internal motion of the methyl group reduces the dipolar effect because of angular averaging, such groups usually have distinct chemical shifts and are easily assigned in solid-state CPMAS  $^{13}\text{C}$  NMR spectra. Although the interrupted decoupling technique is a somewhat phenomenological method and not totally quantitative, the method can effectively increase the resolution one may achieve in  $^{13}\text{C}$ -CPMAS studies. In essence, dipolar dephasing is a very promising spectral editing method for the solid-state.

Figure 19B depicts the spectrum of the PGP after a decoupling delay time of 40  $\mu\text{s}$ . Almost all of the  $^{13}\text{C}$  resonance responses from the carbohydrate portion of the sample have been attenuated or eliminated entirely from the spectrum. Some loss in the signal-to-noise ratio (approximately 25 to 30%) is apparent in such an experiment as would be expected due to some dipolar dephasing of the remaining nonprotonated and methyl resonance signal intensities.  $^{13}\text{C}$  resonances are still evident at 105 ppm and some response is still seen at 75 ppm. When the magnitude of the signal at 75 ppm is compared to that at 150 ppm in Figure 19A, the domination

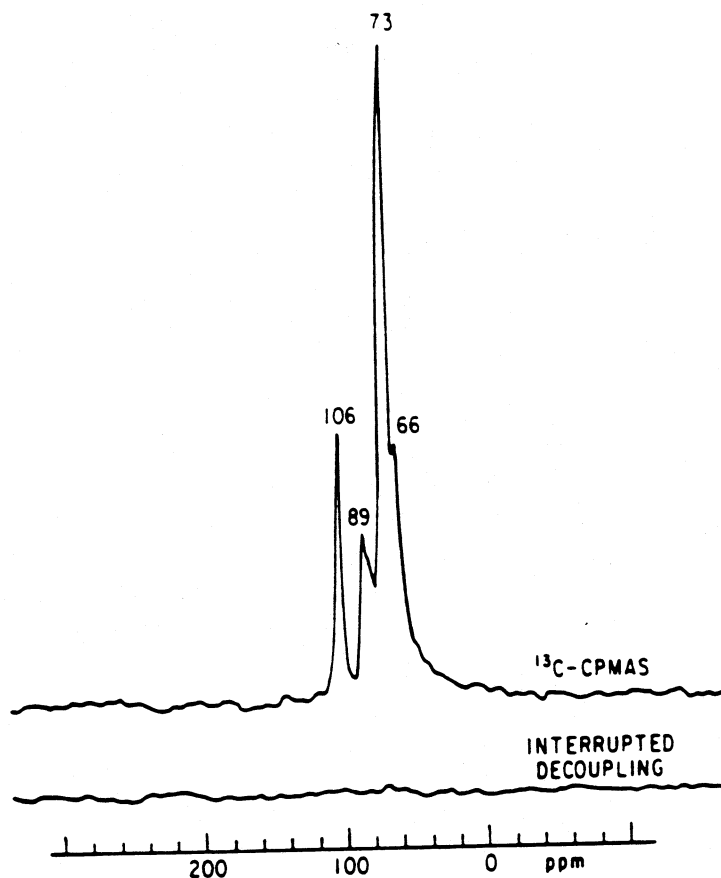


FIGURE 20. Microcrystalline cellulose  $^{13}\text{C}$ -CPMAS spectra. (From Gerasimowicz, W. V., Hicks, K. B., and Pfeffer, P. E., *Macromolecules*, 17, 2597, 1984. With permission.)

of the former is noticed. The 75 ppm resonance is only seen as a residual signal when compared with the 150 ppm resonance in Figure 19B. Therefore, this residual signal is probably from structures that are very low in concentration and does not adversely affect the values of the relaxation times (determined by standard  $T_{1H}$  methodology) for the 75 ppm resonances in Figure 19A. In order to determine whether those residual signals at 75 ppm were from ordered cellulose molecules, a microcrystalline sample (Avicel) was examined under standard  $^{13}\text{C}$ -CPMAS conditions and under identical conditions but with interrupted  $^{13}\text{C}$ - $^1\text{H}$  dipolar dephasing (Figure 20). When the microcrystalline cellulose is examined with dipolar dephasing, no signals are evident either for the cellulose ring or for the anomeric carbon nuclei. Thus, the peaks in Figure 19B at approximately 75 and 105 ppm are not from ordered, crystalline cellulose constituents in the PGP matrix. In several reports of the  $^{13}\text{C}$  NMR solution spectra of lignins, investigators have proposed that  $^{13}\text{C}$  signals between about 102 and 108 ppm have as much likelihood of being due to  $^{13}\text{C}$  resonances from sinapyl structures as from anomeric carbon nuclei of glycosides.<sup>99,100</sup> Thus, the  $^{13}\text{C}$  resonance at 105 ppm in Figure 19B may be associated with lignin polymer, especially due to the corresponding strong intensity at 150 to 155 ppm. Another possible assignment for this resonance could be C-2 nonprotonated carbon nuclei of associated keto sugar polymers. However, the noncarbohydrate and other previously unresolved components are no longer obscured as seen when Figure 19B is compared with Figure 19A. The features that were previously hidden, such as the lignin methoxy at 56 ppm and the aromatic carbon moieties between 130 and 155 ppm, now dominate the spectrum in Figure 19B.

In order to measure the  $T_{1H}$  values for these components, we have combined the  $T_{1H}$  inversion-recovery sequence with the  $^{13}\text{C}$ - $^1\text{H}$  dipolar dephasing mechanism. Under very careful Hartmann-

**Table 7**  
**PICEAE GLAUCA PULP COMPONENT T<sub>1H</sub> RELAXATION**  
**VALUES<sup>a</sup> (INTERRUPTED DECOUPLING)**

[Fe <sup>3+</sup> ] <sup>c</sup>	<sup>13</sup> C chemical shift <sup>b</sup>			
	150	135	74	55
153	36.9	36.5	51.4	42.1
184	23.0	25.7	44.2	30.1
419	23.3	24.7	31.3	27.8
2860	14.1	12.3	17.2	14.3
25400	4.5	5.9	9.2	7.7

<sup>a</sup> ms ± 10%.

<sup>b</sup> ppm.

<sup>c</sup> Concentration in ppm.

From Gerasimowicz, W. V., Hicks, K. B., and Pfeffer, P. E., *Macromolecules*, 17, 2597, 1984. With permission.

**Table 8**  
**RELAXATION VALUES<sup>a</sup> OF PICEAE GLAUCA**  
**PULP<sup>b</sup>**

[Fe <sup>3+</sup> ] <sup>c</sup>	T <sub>1H</sub>	T <sub>10H</sub>	T <sub>CH</sub> <sup>d</sup>
153 <sup>e</sup>	78.8 (82.0) <sup>f</sup>	9.9	0.095
184	79.0 (82.6)	9.2	
419	53.2 (55.9)	7.8	
2860	13.1 (13.8)	6.8	
25400	2.9 (2.9)	2.7	

<sup>a</sup> ms ± 10%.

<sup>b</sup> Carbohydrate region of <sup>13</sup>C spectra at about 75 ppm.

<sup>c</sup> Concentration in ppm.

<sup>d</sup> ±25%.

<sup>e</sup> Iron content of zero-doped *Piceae glauca* pulp.

<sup>f</sup> Values in parentheses represent T<sub>1H</sub> values for anomeric carbohydrate resonances at about 105 ppm.

From Gerasimowicz, W. V., Hicks, K. B., and Pfeffer, P. E., *Macromolecules*, 17, 2597, 1984. With permission.

Hahn matching conditions for spectral acquisition, the T<sub>1H</sub> relaxation values were determined for these now-visible components. The results are listed in Table 7. Unlike the homogeneous relaxation behavior observed for the wood pulp in Table 8, the relaxation of the various resonances is heterogeneous. Proton spin-lattice relaxation effects are not uniform throughout the sample.

Fe<sup>3+</sup> induces shortening of proton spin-lattice relaxation times across the board in homogeneous samples. The residual resonances seen at a <sup>13</sup>C chemical shift of 74 ppm at an Fe<sup>3+</sup> concentration of 153 ppm do not have the same T<sub>1H</sub> as observed for the overall wood pulp carbohydrate seen in Table 8 under the same conditions. This result suggests that these structures may be isolated and different in nature than the majority of the cellulose or hemicellulose previously observed under the normal noninterrupted decoupling conditions. Furthermore,

## WHOLE SAMPLES

## HUMIC SUBSTANCES

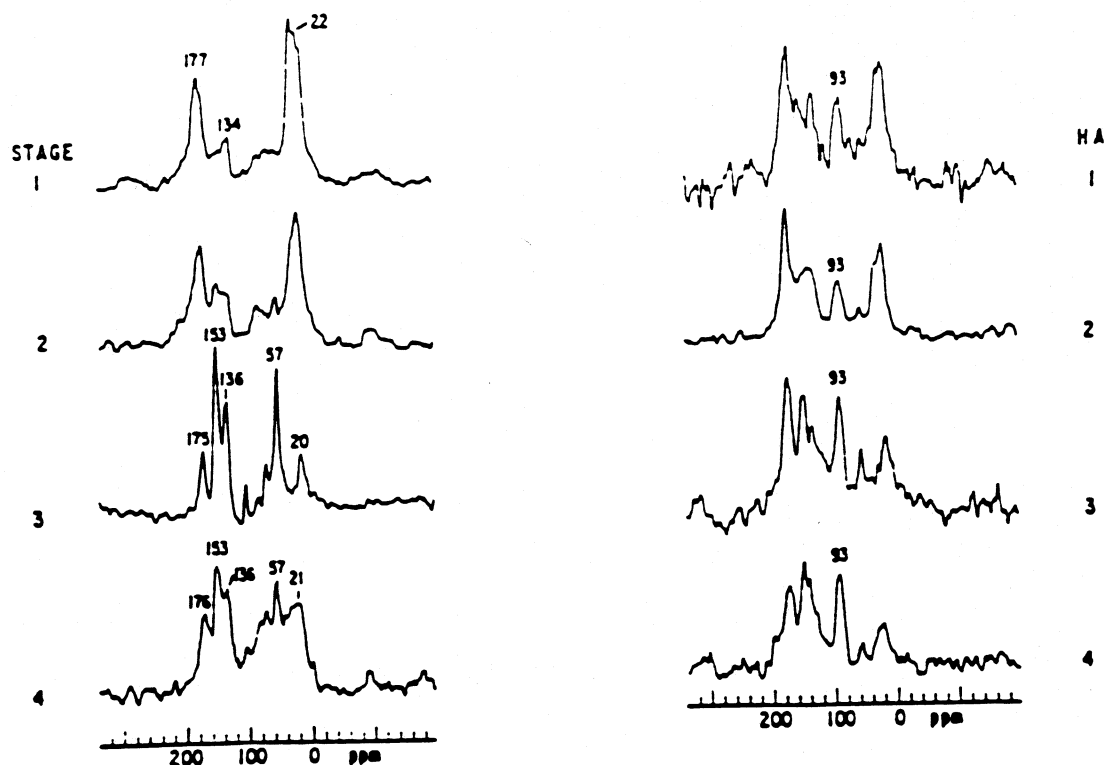


FIGURE 21.  $^{13}\text{C}$ -CPMAS spectra of whole sludges and humic substances with  $^1\text{H}$ - $^{13}\text{C}$  interrupted decoupling. (From Ierasimowicz, W. V. and Byler, D. M., *Soil Sci.*, 139, 270, 1985. With permission.)

These structures may be somewhat more mobile in the solid than more rigid cellulose-like domains resulting in localized attenuation of the  $^{13}\text{C}$ - $^1\text{H}$  dipolar interaction. Such differences in native wood carbohydrate, lignin, and aromatic relaxation times would not be inconsistent with the fact that molecular weight distributions of polysaccharides in typical wood and plant polymers point to their polydisperse nature, as well as their very large size.<sup>101</sup> Zumbulyadis has shown that multicomponent proton relaxation behavior is useful in examining crystalline and amorphous domains in poly(ethylene)terephthalate, and has suggested that proton spin-lattice relaxation times may be used to estimate domain sizes in heterogeneous systems, particularly polymers.<sup>102</sup> Our work extends the utility of this concept to naturally occurring solid heteropolymers.

One final aspect of this system revolves around the data shown in Figure 19C. This figure represents the standard  $^{13}\text{C}$ -CPMAS NMR spectrum of cellulase-treated PGP. A remarkable qualitative similarity is noticeable in the resolvable  $^{13}\text{C}$  chemical shifts when Figure 19B is compared with 19C. Due to their nonprotonated nature ( $\text{OCH}_3$  excepted), the interrupted decoupling technique seems to differentiate the noncarbohydrate components without any chemical or enzymatic degradation of the cellulose. The utility of this method is thus further exemplified.

Another example of this technique is shown in Figure 21. To facilitate comparison, this figure depicts the  $^{13}\text{C}$ -CPMAS spectra of both whole sludge samples and the HAs extracted from these materials.<sup>39,59</sup> One important consideration concerning the spectra shown in Figure 21A is that these data were obtained with no chemical modification whatsoever of the original, whole sample. The interrupted-decoupling technique permits some resolution enhancement of the substituted aromatic and remotely protonated carbon nuclei of the HA components. (See

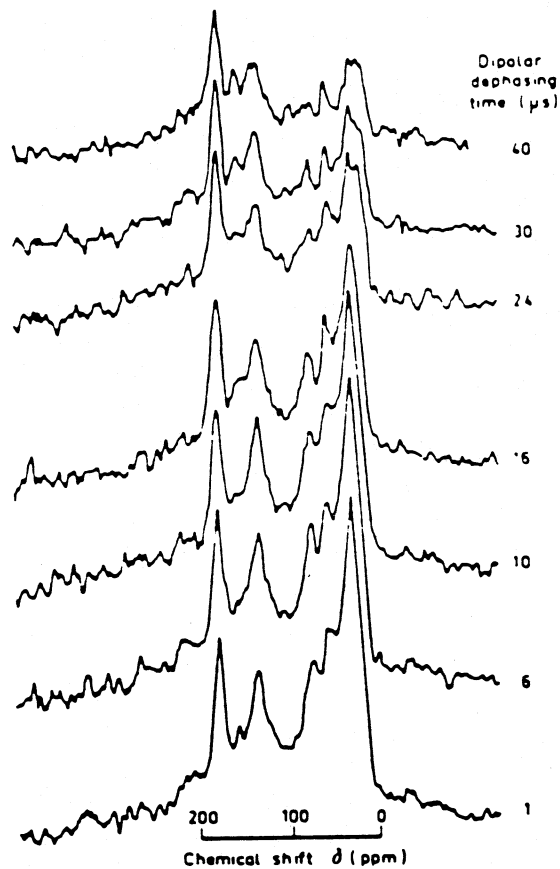


FIGURE 22. Effects of varying the dipolar dephasing time  $T_{DD}$  on spectral features in the NMR spectrum of sedimentary HA. (From Gillam, A. H., Wilson, M. A., and Collin, P. J., *Org. Geochem.*, 11, 91, 1987. With permission.)

specifically the spectral frequency from about 135 to 155 ppm.) One can now more readily discern peaks centered around 153 ppm, which are O- or N-substituted aromatic C nuclei, as well as resonances at approximately 136 ppm, which may be assigned to aromatic or olefinic nuclei that are not electronegatively substituted (Figure 21). The aliphatic, or paraffinic region centered around 22 ppm is also more clearly resolved in all cases shown in Figure 21 than in any of the standard <sup>13</sup>C-CPMAS spectra in Figure 15, for example. The envelope of resonance peaks centered around 22 ppm may also be indicative of carbon-to-carbon branch points, rather than straight-chain methylene groups.

<sup>13</sup>C-<sup>1</sup>H dipolar dephasing NMR has been employed in a structural analysis of sea loch sedimentary humic material.<sup>103</sup> A sea loch is an enclosed, highly productive area along a sea coast. Quite often these areas are fjordic in nature. Increasingly, commercial operations, such as fish farms and paper pulping mills are being established in such areas. Therefore, the natural environment may be disrupted over time. Knowledge of the structure and composition of sedimentary humic substances from sea lochs which have not been polluted or disturbed would be beneficial in establishing the conditions of the habitat at natural equilibrium. Furthermore, one could then assess possible future interactions of the sediment with cellulosic materials.

Such a study has been reported on sediment samples collected from Loch Thurnaig, approximately 1000 m in diameter and semienclosed.<sup>103</sup> The effect of varying the dipolar dephasing time on the NMR spectrum of the humic acid is shown in Figure 22. The resonance at 155 ppm is more prominent, showing nonprotonation. This signal has been attributed to

phenols or an aryl ether functionality. A means of distinguishing between methoxy and amino acid carbon is to study rates of signal loss as a function of interrupted decoupling time. The rate of decay for the resonance at 55 ppm is shorter than that for methoxyl groups alone.<sup>103</sup> Although one cannot rule out the presence of methoxy carbon in this system, certainly unresolved amino acid appears to contribute to that area of the spectrum. However, one must be aware that errors arise in any attempt to quantify carbon types by measurements of this type.<sup>95-98</sup> Aromaticity was found to be higher in the sedimentary HA fraction when compared to the sedimentary fulvic acid fraction. Furthermore, the DOM appeared to resemble marine humic matter more closely than terrestrial derivatives.<sup>103</sup>

Similarly, oil shale deposits can be examined in order to evaluate the potential of such resources. These same spectroscopic techniques have been employed in examining various kerogen concentrates.<sup>104</sup> The NMR was able to distinguish between highly aliphatic Type I algal kerogens and kerogens derived from carbonaceous shales which have significant aromatic carbon fractions and resemble Type III kerogens.<sup>104</sup>

Spectra of the carbonaceous kerogens appear similar to those of lignite which are suggestive of algal and terrestrial sources. The interrupted decoupling spectra reveal oxygen-substituted carbons in the carbonaceous shales. This structural characteristic may be related to its ability to undergo CO<sub>2</sub> evolution at low temperature during heating, and to subsequent conversion levels upon pyrolysis to oil and gas products.<sup>104</sup>

Decomposition of leaves in soil has also been studied by <sup>13</sup>C-NMR with and without interrupted decoupling, as well as chemical structure of fossil leaves.<sup>105</sup> The results show that fossil leaves and rhizomes retain carbohydrates, and on the basis of carbon content, the concentrations of carbohydrate in fossil rhizomes and their living counterparts are similar. Fossilized leaves, however, contain much less carbohydrate than do their living counterparts.<sup>105</sup> The organic matter associated with the fossilized leaves was quite different in structure than the fossilized leaves themselves. This associated organic matter seemed to resemble humic substances.<sup>105</sup> Thus, the leaves and their associated organics may be subject to rather different transformation processes in their natural habitat.

## **B. Some Other Nuclei in CPMAS Studies of Soils**

### *1. <sup>31</sup>P NMR Studies in Soil Systems*

Several examples of <sup>31</sup>P-CPMAS spectra of whole soils have now appeared in the literature. In 1981, Williams reported a <sup>31</sup>P spectrum of whole soil.<sup>106</sup> Recently Frye has published <sup>31</sup>P-CPMAS spectra of HAs and fulvic acids.<sup>107</sup> These spectra are shown in Figures 23 and 24.<sup>107</sup> The authors concluded that the single pulse spectra (those acquired with MAS and high-power decoupling but without CP) are as easily acquired as the CP data. However, the overall spectral resolution is still very poor. Thus, difficulties remain in the interpretation of such spectra due to line broadening. The broadening effects may be caused by heterogeneity inherent in the samples themselves.

Turner et al. have obtained high-resolution MAS <sup>31</sup>P-NMR spectra of a variety of orthophosphates.<sup>108</sup> Table 9 shows a listing of the compounds, chemical shift ranges, average P-O bond length, and other information is tabulated. These workers were able to develop an empirical correlation between the isotropic chemical shift and  $Z\sqrt{r}$ , where Z is the cationic charge and r is the cationic radius.<sup>108</sup>

Many of the compounds displayed rather small chemical shift anisotropies, and many of the spectra were dominated by the main isotropic peak (see Figure 25).<sup>108</sup> The CSA was demonstrated to vary in an approximately linear fashion with P-O bond length, and with the deviation of the O-P-O bond angle from tetrahedral.<sup>108</sup>

Such model systems may prove useful in testing phosphate bonding in soils and other heterogeneous or amorphous systems. Clearly however, better resolution in the <sup>31</sup>P spectra of soils must be achieved first in order to apply the techniques described. Thus, <sup>31</sup>P-CPMAS, although possible, is still not nearly as useful as <sup>13</sup>C-CPMAS in the analysis of soils. However,

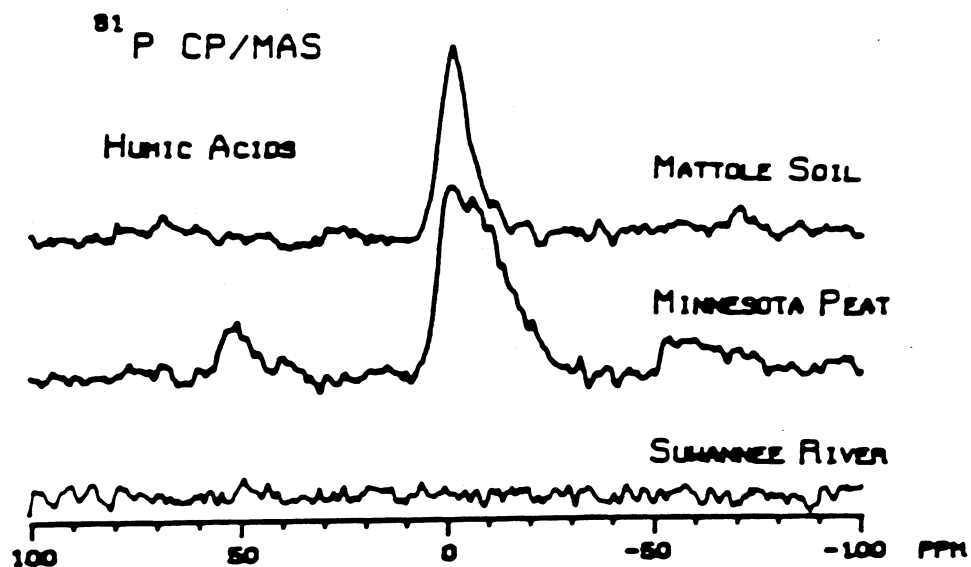


FIGURE 23.  $^{31}\text{P}$ -CPMAS spectra of HAs. Approximately 10,000 scans were taken on a modified Nicolet NT-150 spectrometer, using a 2-ms CT, 2-s repetition time, and a spinning rate of 3.5 kHz. (From Frye, J. S., Bonnimann, C. E., and Maciel, G. E., *NMR of Humic Substances and Coal*, Wershaw, W. L. and Makita, M. A., Eds., Lewis Publishers, Chelsea, MI, 1987, 33. With permission.)

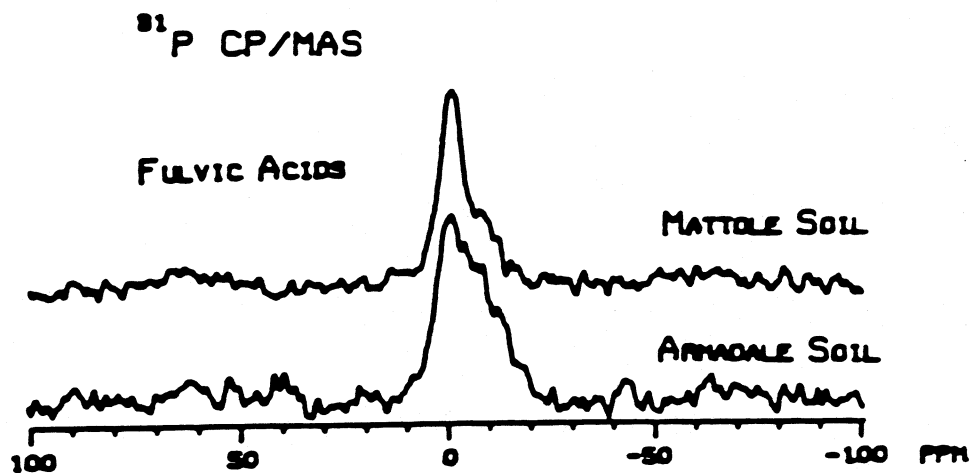


FIGURE 24.  $^{31}\text{P}$ -CPMAS spectra of fulvic acids. Experimental conditions as in Figure 23. (From Frye, J. S., Bonnimann, C. E., and Maciel, G. E., *NMR of Humic Substances and Coal*, Wershaw, W. L. and Makita, M. A., Eds., Lewis Publishers, Chelsea, MI, 1987, 33. With permission.)

direct observation of the  $^{31}\text{P}$  nuclei and small differences between samples is feasible and adds another tool to the arsenal of the soil scientist.

## 2. $^{15}\text{N}$ NMR Studies in Soil Systems

$^{15}\text{N}$ -CPMAS NMR studies of enriched humic soil components and  $^{15}\text{N}$ -labeled melanoidins have appeared.<sup>109,110</sup> Figure 26 depicts  $^{15}\text{N}$ -CPMAS spectra of these substances. The three  $^{15}\text{N}$ -CPMAS NMR spectra of the melanoidins and the HA show a predominant peak at 97 ppm. This resonance is characteristic of nitrogen from secondary amide structures. The band at 155 ppm is due to pyrrolelike nitrogen, and the 128 band can be assigned either to a pyrrole or secondary amide structure and to indole nitrogen.  $^{15}\text{N}$ -NMR (thus far) has only shown utility where isotopic enrichment has been performed.  $^{15}\text{N}$  at natural abundance is not yet very promising due to the

**Table 9**  
**<sup>31</sup>P-NMR AND STRUCTURE PARAMETERS**

<sup>31</sup>P shifts in orthophosphates

Compound	$\delta_1$ (ppm)	$\delta_{11}$ (ppm)	$\delta_{22}$ (ppm)	$\delta_{33}$ (ppm)	$ \Delta\delta $ (ppm)	$r_{P-O}^*$ (Å)	$\frac{\sum  109.5 - \delta_i }{n}$	$n_r$	Ref. <sup>b</sup>
NH <sub>4</sub> H <sub>2</sub> PO <sub>4</sub>	0.9	-15.4	-5.6	23.6	34.1	1.537	1.17	1.23	17
(NH <sub>4</sub> ) <sub>2</sub> HPO <sub>4</sub>	1.5	-33.6	-9.9	48.0	69.8	1.539	2.38	1.23	18
Li <sub>3</sub> PO <sub>4</sub>	10.8	NM <sup>c</sup>	NM	NM	NM	1.546	0.68	1.17	19
Na <sub>3</sub> PO <sub>4</sub> ·12H <sub>2</sub> O	7.8	NM	NM	NM	NM	1.526	0.15	1.19	20
NaH <sub>2</sub> PO <sub>4</sub> ·H <sub>2</sub> O	2.3	61.1	23.1	-77.3	119.4	1.552	3.87	1.23	21
Na <sub>2</sub> HPO <sub>4</sub>	6.6	-48.9	-5.7	74.5	101.8	1.550	3.17	1.20	22
NaNH <sub>4</sub> HPO <sub>4</sub> ·4H <sub>2</sub> O	5.1	-36.9	-4.2	56.5	77.0	1.541	2.73	1.21	23
KH <sub>2</sub> PO <sub>4</sub>	4.3	-15.6	3.9	24.8	30.4	1.538	0.925	1.21	24, 25
K <sub>2</sub> HPO <sub>4</sub> ·3H <sub>2</sub> O	2.1	-45.0	-6.5	57.8	83.6	NA <sup>d</sup>	NA	1.23	—
Be <sub>3</sub> (PO <sub>4</sub> ) <sub>2</sub>	-9.2	NM	NM	NM	NM	NA	NA	—	—
Mg <sub>3</sub> (PO <sub>4</sub> ) <sub>2</sub> ·8H <sub>2</sub> O	4.6	NM	NM	NM	NM	1.538	0.53	1.21	26
Ca <sub>3</sub> (PO <sub>4</sub> ) <sub>2</sub>	3.0	NM	NM	NM	NM	1.531	2.51	1.22	27
CaHPO <sub>4</sub>	-0.6	NM	NM	NM	NM	1.541	21.0	1.24	28
BaHPO <sub>4</sub>									
Site 1	-0.5	-40.9	-7.8	47.3	71.7	NA	NA	1.24	—
Site 2	-2.8	-39.1	-14.9	45.7	72.7	NA	NA	1.26	—
BPO <sub>4</sub>	-29.5	NM	NM	NM	NM	NA	NA	1.43	—
AlPO <sub>4</sub>	-24.5	NM	NM	NM	NM	1.516	0.70	1.40	29
GaPO <sub>4</sub>	-9.8	NM	NM	NM	NM	1.56	NA	1.30	30
YPO <sub>4</sub>	-0.9	NM	NM	NM	NM	1.50	NA	1.25	31
LaPO <sub>4</sub> ·nH <sub>2</sub> O	-3.3	NM	NM	NM	NM	NA	NA	1.26	—
P <sub>2</sub> O <sub>5</sub> ·24WO <sub>3</sub> ·nH <sub>2</sub> O	-15.1	NM	NM	NM	NM	NA	NA	1.34	—

\* Average P-O bond length.

<sup>b</sup> Structure reference.

<sup>c</sup> NM, not measured.

<sup>d</sup> NA, not available.

From Turner, G. L., Smith, K. A., Kirkpatrick, R. J., and Oldfield, E., *J. Magn. Reson.*, 70, 408, 1986. With permission.

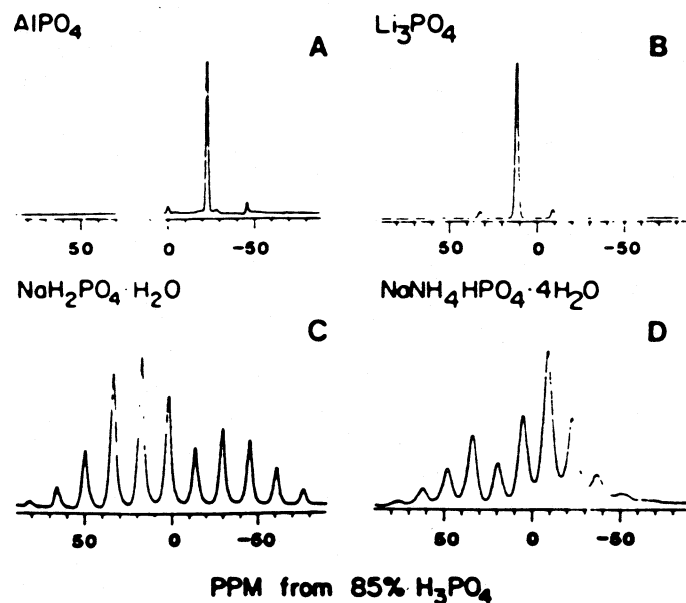


FIGURE 25. Representative  $^{31}\text{P}$ -NMR spectra of several orthophosphates. (A)  $\text{AlPO}_4$ , 4.6 kHz MASS, 20 scans, 4- $\mu\text{s}$  pulse (20° flip angle). (B)  $\text{Li}_3\text{PO}_4$ , 4.2 kHz MASS, 444 scans, 9- $\mu\text{s}$  pulse (45° flip angle). (C)  $\text{NaH}_2\text{PO}_4 \cdot \text{H}_2\text{O}$ , 3.2 kHz MASS, 60 scans, 9- $\mu\text{s}$  pulse (45° flip angle). (D)  $\text{NaNH}_4\text{HPO}_4 \cdot 4\text{H}_2\text{O}$ , 2.8 kHz MASS, 28 scans, 9- $\mu\text{s}$  pulse (45° flip angle). All spectra were recorded using a sweep width of 36.4 kHz, a 10-s recycle time, 10-Hz Gaussian line broadening, and  $^1\text{H}$  dipolar decoupling was routinely applied for all systems. (From Turner, G. L., Smith, K. A., Kirkpatrick, R. J., and Oldfield, E., *J. Magn. Reson.*, 70, 408, 1986. With permission.)

low natural abundance of this species (0.37%). Very little signal is available at such levels. Furthermore, the relative sensitivity of  $^{15}\text{N}$  (due to its small magnetogyric ratio) as compared with proton is only about 0.1%. Therefore, the Hartmann-Hahn matching or CP condition is difficult to achieve under the high-power conditions of the CPMAS experiment.

### 3. High-Resolution Solid-State Proton NMR of Soil Materials

Just as solid-state NMR studies of  $^{13}\text{C}$  and other nuclei have been stimulated by the availability of CPMAS spectrometers and technology, sophisticated pulse sequences have also been developed to observe  $^1\text{H}$ s in solids.<sup>111,112</sup> The technique employed is known as combined rotation and multiple pulse spectroscopy (CRAMPS). A full exposition of the theory behind this method is beyond the scope of this paper. Suffice it to say that the large homonuclear couplings among protons in solids can be reduced to manageable levels by means of the CRAMPS experiment in certain cases. Figures 27 and 28 illustrate the only spectra in the literature of such a type on soils with which we are familiar.<sup>107</sup> Quantitation (integration of signal areas) is still not very accurate. However, some boundary conditions can now be placed on the proton distribution and environment in soils by solid state means. The CRAMPS method is subject to certain advantages and limitations. Advantages include the fact that protons afford high sensitivity due to their natural abundance and large magnetogyric ratios. Fewer spinning side bands are apparent thus causing less overlap with isotropic resonance positions. Disadvantages include more severe hardware requirements, smaller sample size, and smaller rotors for these experiments. The spectra presented indicate the potential for qualitative analysis at the very minimum.

### 4. Oxygen-17 and Other Nuclei

Oxygen-17 is now being actively pursued as a probe, and is being used to study the structure

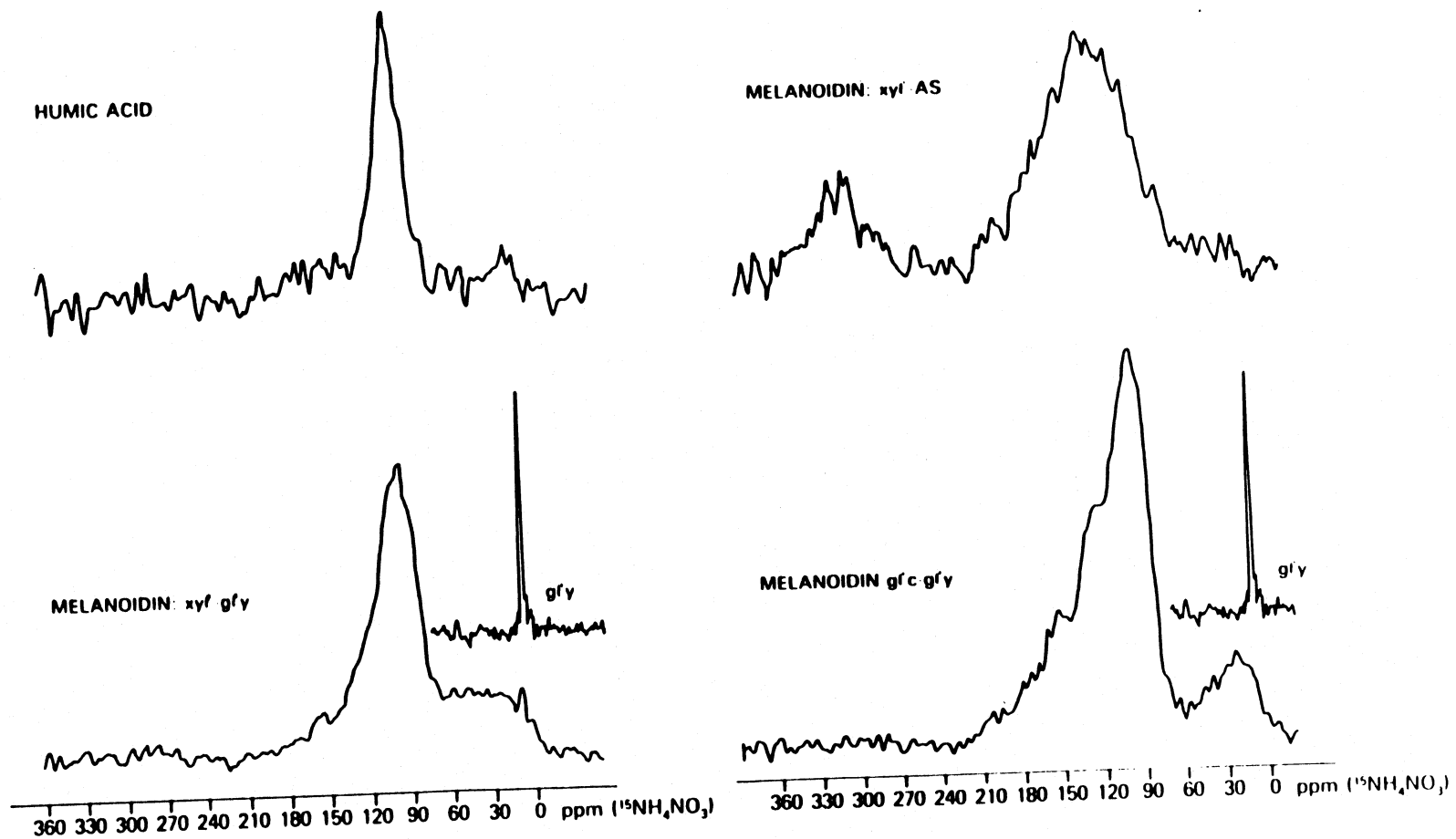


FIGURE 26.  $^{15}\text{N}$ -CPMAS spectra of  $^{15}\text{N}$ -labeled HA and melanoindins 1 (Xyl-Gly), 2 (Gly-Gly), 3 (Xyl-AS). Spectrum of glycine- $^{15}\text{N}$  is shown as an insert. (From Benzing-Purdie, L., Ripmeester, J. A., and Preston, C., *J. Agric. Food Chem.*, 31, 913, 1983. With permission.)

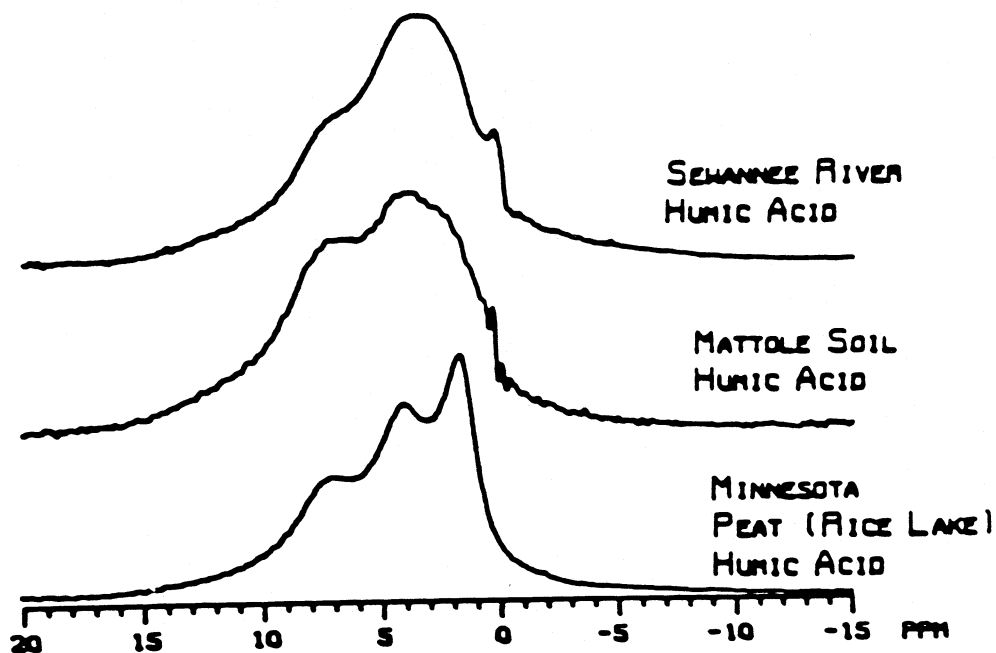


FIGURE 27.  $^1\text{H}$  CRAMPS spectra of HAs. 500 scans were taken. (From Frye, J. S., Bonnimann, C. E., and Maciel, G. E., *NMR of Humic Substances and Coal*, Wershaw, W. L. and Makita, M. A., Eds., Lewis Publishers, Chelsea, MI, 1987, 33. With permission.)

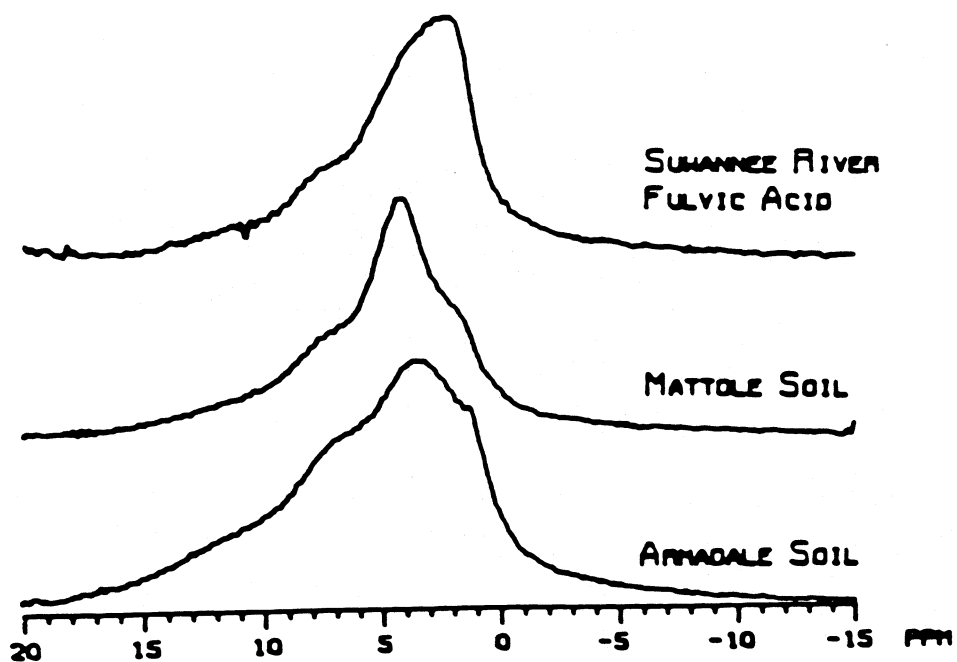


FIGURE 28.  $^1\text{H}$  CRAMPS spectra of fulvic acids. Experimental conditions as for Figure 27. (From Frye, J. S., Bonnimann, C. E., and Maciel, G. E., *NMR of Humic Substances and Coal*, Wershaw, W. L. and Makita, M. A., Eds., Lewis Publishers, Chelsea, MI, 1987, 33. With permission.)

and reactivity of inorganic solids, glasses, catalysts, ceramics, and minerals. This NMR-active nuclide has an  $I = 5/2$ , a natural abundance of 0.037%, and a magnetogyric ratio of  $-0.5793 \text{ KH/g}$ . G. Walter et al. have recently reported results on a series of CP experiments on  $^{17}\text{O}$ -label inorganic solids.<sup>113</sup>  $^{17}\text{O}$  spectra were obtained on  $\text{Mg}(\text{OH})_2$ ,  $\text{Ca}(\text{OH})_2$ , boehmite ( $\text{AlO}(\text{OH})$ ), tal ( $\text{Mg}_3\text{Si}_4\text{O}_{10}(\text{OH})_2$ ),  $(\text{C}_6\text{H}_5)_3\text{SiOH}$ , and amorphous  $\text{SiO}_2$ .<sup>113</sup>

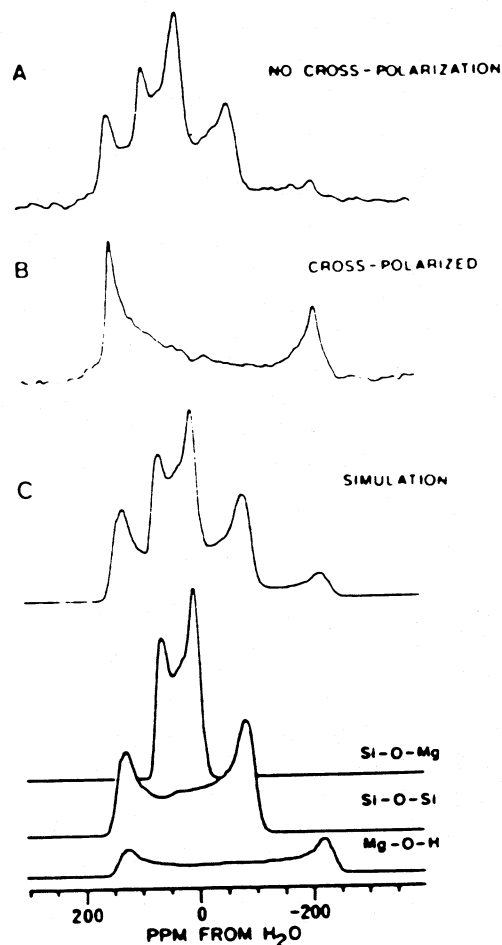


FIGURE 29. Static  $^{17}\text{O}$ -NMR spectra of polycrystalline talc ( $\text{Mg}_3\text{Si}_4\text{O}_{10}(\text{OH})_2$ ) obtained at 67.8 MHz. (A) Proton-decoupled spectrum without CP: 500 scans, 10-s recycle time. (B) Cross-polarized spectrum: 500 scans, 33- $\mu\text{s}$  CT, 10-s recycle time. (C) Simulated spectrum using three second-order quadrupolar powder patterns with the following parameters: (1)  $e^2qQ/h = 3.2$  MHz,  $\nu = 0$ ,  $\delta_i = 40$  ppm, relative intensity, 2.0; (2)  $e^2qQ/h = 5.8$  MHz,  $\nu = 0$ ,  $\delta_i = 50$  ppm, relative intensity 3.0; (3)  $e^2qQ/h = 7.3$  MHz,  $\nu = 0$ ,  $\delta_i = 0$  ppm, relative intensity 1.0. (From Walter, T. W., Turner, G. L., and Oldfield, E., *J. Magn. Reson.*, 76, 106, 1988. With permission.)

Spectra of the mineral talc are shown in Figure 29. The ratio of chemically distinct oxygen sites is 2:3:1 and corresponds to Si-O-Mg, Si-O-Si, and Mg-O-H. The nuclear quadrupole coupling constant ( $e^2qQ/h$ ) and the asymmetry parameter of the electric field gradient tensor, and the isotropic chemical shift are sensitive to the environment. Although Figure 29A shows overlapping powder patterns, the authors were able to simulate three axially symmetric second-order quadrupolar powder patterns (2:3:1 ratio) as seen in Figure 29C.<sup>113</sup> Furthermore, Figure 29B shows how CP can be used to observe hydroxyl groups even when the spectra suffer from extensive overlap. In this same paper, the authors point out methods of spectral "editing" by means of differences in cross-relaxation ratios, and selective observation of resonances from surface hydroxy groups that are rather difficult (or impossible) to detect by conventional  $^{17}\text{O}$  NMR.

The subject of solid-state NMR of clays and mineral systems is another treatise unto itself. For further information on  $^{27}\text{Al}$  and  $^{29}\text{Si}$  solid-state NMR in clays and minerals see Reference 33.

The nuclei and techniques are simply pointed out as potentially applicable to whole soil systems themselves.

### III. CONCLUSIONS

The current explosion in new NMR developments, hardware, software, and pulse sequences is producing a rapid acceleration in the ability of the capable spectroscopist to perform complex solid-state experiments on soils. Structure and a variety of nuclei can easily be examined as well as the dynamics within soil matrices. However, the NMR scientist still needs very well-characterized samples as a basis upon which to interpret his spectra. Over the next 10 years, a combination of NMR and advanced wet chemical techniques should be explored in order to fully exploit and discover the vast amount of information yet untapped in these complex, heterogeneous, environmental matrices.

### REFERENCES

1. Mehring, M., *High Resolution NMR in Solids*, 2nd. ed., Springer-Verlag, Berlin, 1983.
2. Slichter, C. P., *Principles of Magnetic Resonance*, Springer-Verlag, Berlin, 1978.
3. Haeblerlen, U., High Resolution NMR in Solids. Selective Averaging, in *Advances in Magnetic Resonance*, Supplement 1, Waugh, J., Ed., Academic Press, New York, 1976.
4. Gerstein, B. C. and Dybowski, C. R., *Transient Techniques in NMR of Solids*, Academic Press, Orlando, FL, 1985.
5. Abragam, A., *The Principles of Nuclear Magnetism*, Clarendon Press, Oxford, 1961.
6. Hartmann, S. R. and Hahn, E. L., Nuclear double resonance in the rotating frame, *Phys. Rev.*, 128, 2042, 1962.
7. Lurie, F. M. and Slichter, C. P., Spin temperature in nuclear double resonance, *Phys. Rev.*, 133, A1108, 1964.
8. Slusher, R. E. and Hahn, E. L., Sensitive detection of nuclear quadrupole interactions in solids, *Phys. Rev.*, 166, 332, 1968.
9. Redfield, A. G., Pure nuclear electric quadrupole resonance in impure copper, *Phys. Rev.*, 130, 589, 1963.
10. Kaplan, D. E. and Hahn, E. L., Experience de double irradiation en resonance magnetique par la methode d'impulsions, *J. Phys. Radium*, 19, 821, 1958.
11. Yannoni, C. S., High resolution NMR in solids: the CPMAS experiment, *Acc. Chem. Res.*, 15, 201, 1982.
12. Pines, A., Gibby, M. G., and Waugh, J. S., Proton-enhanced NMR of dilute spins in solids, *J. Chem. Phys.*, 59, 569, 1973.
13. O'Donnell, D. J., Bartuska, V. J., Palmer, A. R., and Sindorf, D. W., Modern NMR techniques for solid samples, *Am. Lab.*, 104, 1986.
14. Pfeffer, P. E., High resolution solid state <sup>13</sup>C NMR and its applications in carbohydrate chemistry, *J. Carbohydr. Chem.*, 3, 613, 1984.
15. Andrew, E. R., Magic angle spinning in solid state NMR spectroscopy, *Philos. Trans. R. Soc. London, Ser. A*, 299, 505, 1981.
16. Andrew, E. R., Hinshaw, W. S., and Jasinski, A., High-resolution NMR spectra in the solid state, *Chem. Phys. Lett.*, 24, 399, 1974.
17. Andrew, E. R., Hinshaw, W. S., Hutchins, M. G., and Jasinski, A., A nuclear magnetic resonance investigation of solid tetraphosphorus trisulphide, *Proc. R. Soc. London, Ser. A*, 364, 553, 1978.
18. Andrew, E. R., Bradbury, A., and Eades, R. G., Nuclear magnetic resonance spectra from a crystal rotated at high speed, *Nature*, 182, 1659, 1958.
19. Andrew, E. R., Bradbury, A., and Eades, R. G., Removal of dipolar broadening of nuclear magnetic resonance spectra of solids by specimen rotation, *Nature*, 183, 1802, 1959.
20. Lowe, I. J., Free induction decays of rotating solids, *Phys. Rev. Lett.*, 2, 285, 1959.
21. Andrew, E. R., *Nuclear Magnetic Resonance in Rapidly Rotating Solids*, Coogan, C. K., Ham, N. S., Stuart, S. N., Pilbrow, J. R., and Wilson, G. H. H., Eds., Plenum Press, New York, 1970, 163.
22. Schaefer, J. and Stejskal, E. O., Carbon-13 nuclear magnetic resonance of polymers spinning at the magic angle, *J. Am. Chem. Soc.*, 98, 1031, 1976.

23. Schaefer, J., Stejskal, E. O., and Buchdahl, R., Magic-angle carbon-13 NMR analysis of motion in solid glassy polymers. *Macromolecules*, 10, 384, 1977.
24. Gerstein, B. C., Pembleton, R. G., Wilson, R. C., and Ry, L. M., High resolution NMR in randomly oriented solids with homonuclear dipolar broadening: combined multiple pulse NMR and magic angle spinning. *J. Chem. Phys.*, 66, 362, 1977.
25. Jelinski, L. W., NMR of plastics. *Chemtech*, March 1986, 188.
26. Barron, P. F., Wilson, M. A., Stephens, J., Cornell, B. A., and Tate, K. R., Cross-polarization  $^{13}\text{C}$  NMR spectroscopy of whole soils. *Nature*, 286, 585, 1981.
27. Wilson, M. A., and Goh, G. M., Proton-decoupled pulse Fourier-transform  $^{13}\text{C}$  nuclear magnetic resonance of soil organic matter. *J. Soil Sci.*, 28, 645, 1977.
28. Barron, P. F. and Wilson, M. A., Humic soil and coal structure with magic-angle spinning carbon-13 CP-NMR. *Nature*, 289, 275, 1981.
29. Preston, C. M. and Ripmeester, J. A., Application of solution and solid-state  $^{13}\text{C}$  NMR to four organic soils, their humic acids, fulvic acids, humins, and hydrolysis residues. *Can. J. Spectrosc.*, 27, 100, 1982.
30. Preston, C. M., Mathur, S. P., and Rauthan, B. S., The distribution of copper, amino compounds, and humus fractions in organic soils of differing copper contents. *Soil Sci.*, 131, 344, 1981.
31. Wilson, M. A., Barron, P. F., and Goh, K. M., Differences in structure of organic matter in two soils as demonstrated by  $^{13}\text{C}$  cross-polarization nuclear magnetic resonance spectroscopy with magic angle spinning. *Geoderma*, 26, 323, 1981.
32. Wilson, M. A., Pugmire, R. J., Zilm, K. W., Goh, K. M., Heng, S., and Grant, D. M., Cross-polarization  $^{13}\text{C}$ -NMR spectroscopy with magic angle spinning characterizes organic matter in whole soils. *Nature*, 294, 648, 1981.
33. Fyfe, C. A., *Solid-State NMR for Chemists*. CFC Press, Guelph, Ontario, 1983, 272.
34. Schaefer, J., Stejskal, E. O., and Buchdahl, R., Magic-angle carbon-13 NMR analysis of motion in solid polycarbonate. *J. Macromol. Sci., Phys.*, B13, 665, 1977, and references cited therein.
35. Fyfe, C. A., Mossburger, H., and Yannoni, C. S., A simple magic-angle spinning apparatus for routine use in NMR spectroscopy of solids. *J. Magn Reson.*, 36, 61, 1979.
36. Stejskal, E. O., Schaefer, J., and Waugh, J. S., Magic-angle spinning and polarization transfer in proton enhanced NMR. *J. Magn. Reson.*, 28, 105, 1977.
37. VanderHart, D. L. and Retcovsky, H. L., Estimation of coal aromaticities by proton-decoupled carbon-13 magnetic resonance spectra of whole coals. *Fuel*, 55, 202, 1976.
38. Bartuska, V. J., Maciel, G. E., Schaefer, J., and Stejskal, E. O., Prospects for carbon-13 nuclear magnetic resonance analysis of solid fossil fuel materials. *Fuel*, 56, 345, 1977.
39. Pfeffer, P. E., Gerasimowicz, W. V., and Piotrowski, E. G., Effect of paramagnetic iron on quantitation in carbon-13 cross-polarization magic angle spinning nuclear magnetic resonance spectrometry of heterogeneous environmental matrices. *Anal. Chem.*, 56, 734, 1984.
40. Ganapathy, A. N. and McDowell, C. A., Paramagnetic doping as an aid in obtaining high-resolution carbon-13 NMR spectra of biomolecules in the solid state. *J. Am. Chem. Soc.*, 103, 6011, 1981.
41. Brown, C. E., Effects of chemical modification and cobalt (II) chloride addition on the carbon-13 NMR spectra of carnosine as a solid powder. *J. Am. Chem. Soc.*, 104, 5608, 1982.
42. Sullivan, M. J. and Maciel, G. E., Structural resolution in the carbon-13 nuclear magnetic resonance spectrometric analysis of coal by cross-polarization and magic-angle spinning. *Anal. Chem.*, 54, 1610, 1982.
43. Earl, W. L. and VanderHart, D. L., Observations in solid polyethylene by carbon-13 nuclear magnetic resonance with magic angle spinning. *Macromolecules*, 12, 762, 1979.
44. Yoshida, T., Maekawa, Y., and Fujita, T., Cross-polarization and magic angle spinning carbon-13 nuclear magnetic resonance spectrometry for quantitative analysis of coal and coal-derived solids. *Anal. Chem.*, 55, 388, 1983.
45. Gerstein, B. C., Ryan, M. L., and Murphy, P. D., A tentative identification of average aromatic ring size in an Iowa vitrain and a Virginia vitrain. *Prepr. Pap., Am. Chem. Soc., Div. Fuel Chem.*, American Chemical Society, Washington, D.C., 24, 90, 1979.
46. Preston, C. M., Dudley, R. L., Fyfe, C. A., and Mathur, S. P., Effects of variations in contact times and copper contents in a  $^{13}\text{C}$  CPMAS study of samples of four organic soils. *Geoderma*, 33, 245, 1984.
47. Lowe, L. E., Carbohydrate. in *Soil Organic Matter*. Schnitzer, M. and Khan, S. U., Eds., Elsevier, New York, 1978, 65.
48. Rendlemann, J., Jr., Complexes of alkali metals and alkaline-earth metals with carbohydrates. *Adv. Carbohydrate Chem.*, 21, 209, 1966.
49. Wilson, M. A., Applications of NMR spectroscopy to the study of the structure of soil organic matter. *J. Soil Sci.*, 32, 167, 1981.
50. Hatcher, P. G., Berger, I. A., Dennis, L. W., and Maciel, G. E., Solid-state  $^{13}\text{C}$  NMR of sedimentary humic substances: new revelations on their chemical composition. in *Aquatic and Terrestrial Humic Materials*. Christman, R. F. and Gjessing, E. T., Eds., Ann Arbor Science, Ann Arbor, MI, 1983, 37.

51. **Lindberg, J. J. and Hortling, B.**, Cross-polarization magic-angle spinning NMR studies of carbohydrates and aromatic polymers. *Adv. Polymer Sci.*, 1, 66, 1985.
52. **Hatcher, P. G., Breger, I. A., Maciel, G. E., and Szeverenyi, N. M.**, Geochemistry of humin, in *Humic Substances in Soil, Sediment, and Water*, Aiken, G. R., McKnight, D. M., Wershaw, R. L., and MacCarthy, P., Eds., John Wiley & Sons, New York, 1985, 275
53. **Wershaw, R. L.**, Applications of NMR spectroscopy for determining functionality in humic substances, in *Humic Substances in Soil, Sediment, and Water*, Aiken, G. R., McKnight, D. M., Wershaw, R. L., and MacCarthy, P., Eds., John Wiley & Sons, New York, 1985, 561.
54. **Kononova, M. M.**, *Soil Organic Matter*, Pergamon Press, Oxford, 1966.
55. **Forsman, J. P.**, Geochemistry of kerogen, in *Organic Geochemistry*, Berger, I. A., Ed., Pergamon Press, Oxford, 1963, 148.
56. **Steurmer, D. H., Kaplan, I. R., and Peters, K. E.**, Source indicators of humic substances and proto-kerogen: stable isotopic ratios, elemental compositions and electron spin resonance spectra. *Geochim. Cosmochim. Acta*, 42, 989, 1978.
57. **Hatcher, P. G., Rowan, R., and Mattingly, M. A.**, <sup>1</sup>H and <sup>13</sup>C NMR of marine humic substances. *Org. Geochem.*, 2, 77, 1980.
58. **Hatcher, P. G., Maciel, G. E., and Dennis, L. W.**, Aliphatic structure of humic acids: a clue to their origin. *Org. Geochem.*, 3, 43, 1981.
59. **Gerasimowicz, W. V. and Byler, D. M.**, Carbon-13 CPMAS NMR and FTIR spectroscopic studies of humic acids. *Soil Sci.*, 139, 270, 1985.
60. **Gerasimowicz, W. V., Byler, D. M., and Piotrowski, E. G.**, Infrared spectroscopic characterization of sludges and sludge extracts: comparison of several mild extraction procedures. *Soil Sci.*, 136, 237, 1983.
61. **Hatcher, P. G., Schnitzer, M., Dennis, L. W., and Maciel, G. E.**, Aromaticity of humic substances in soils. *J. Soil Sci. Soc. Am.*, 45, 1089, 1094, 1981.
62. **Dalal, R. C. and Mayer, R. J.**, Long term trends in Fertility of soils under continuous cultivation and cereal cropping in southern Queensland. I. Overall changes in soil properties and trends in winter cereal yields. *Aust J. Soil Res.*, in press.
63. **Dalal, R. C. and Mayer, R. J.**, Long term trends in fertility of soils under continuous cultivation and cereal cropping in Southern Queensland. II. Total organic carbon and its rate of loss from the soil profile. *Aust. J. Soil Res.*, in press.
64. **Skjemstad, J. O., Dalal, R. C., and Barron, P. F.**, Spectroscopic investigations of cultivation effects on organic matter of vertisols. *Soil Sci. Soc. Am. J.*, 50, 354, 1986.
65. **Catroux, G. and Schnitzer, M.**, Chemical, spectroscopic, and biological characteristics of the organic matter in particle size fractions separated from an Aquoll. *Soil Sci. Soc. Am. J.*, 51, 1200, 1987.
66. **Skjemstad, J., Frost, R. L., and Barron, P. F.**, Structural units in humic acids from South-Eastern Queensland soils as determined by <sup>13</sup>C-NMR spectroscopy. *Aust. J. Soil Res.*, 21, 539, 1983.
67. **Wilson, M. A., Goh, K. M., Collin, P. J., and Greenfield, L. G.**, Origins of humus variation. *Org. Geochem.*, 9, 225, 1986.
68. **Christman, R. F. and Gjessing, E.**, Priorities in humic research, in *Aquatic and Terrestrial Humic Materials*, Christman, R. F. and Gjessing, E., Eds., Ann Arbor Science, Ann Arbor, MI, 1983, 517.
69. **Horne, R. A.**, *Marine Chemistry*, Wiley Interscience, New York, 1969, 229.
70. **Gillman, A. H. and Wilson, M. A.**, Application of <sup>13</sup>C-NMR spectroscopy to the structural elucidation of dissolved marine humic substances and their phytoplanktonic precursors in aquatic and terrestrial humic materials. Christman, R. F. and Gjessing, E., Eds., Ann Arbor Science, Ann Arbor, MI, 1983, 25.
71. **Gillman, A. H. and Wilson, M. A.**, Pyrolysis-GC-MS and NMR studies of dissolved seawater humic substances and isolates of a marine diatom. *Org. Geochem.*, 8, 15, 1985.
72. **Orem, W. H. and Hatcher, P. G.**, Solid-State <sup>13</sup>C-NMR studies of dissolved organic matter in pore waters from different depositional environments. *Org. Geochem.*, 11, 73, 1987.
73. **Lenheer, J. A., Wilson, M. A., and Malcolm, R. L.**, Presence and potential significance of aromatic-ketone groups in aquatic humic substances. *Org. Geochem.*, 11, 273, 1987.
74. **Schnitzer, M. and Preston, C. M.**, Analysis of humic acids by solution and solid-state carbon-13 nuclear magnetic resonance. *Soil Sci. Soc. Am. J.*, 50, 326, 1987.
75. **Ogner, G.**, A comparison of four different raw humus types in Norway using chemical degradations and CPMAS <sup>13</sup>C-NMR spectroscopy. *Geoderma*, 16, 343, 1985.
76. **Wilson, M. A., Vassallo, A. M., Perdue, E. M., and Reuter, J. H.**, Compositional and solid-state nuclear Magnetic resonance study of humic and fulvic acid fractions of soil organic matter. *Anal. Chem.*, 59, 551, 1987.
77. **Vassallo, A. M., Wilson, M. A., Collin, P. J., Oades, J. M., and Waters, A. G.**, Structural analysis of geochemical samples by solid-state nuclear magnetic resonance spectrometry. Role of paramagnetic material. *Anal. Chem.*, 59, 558, 1987.
78. **Saiz-Jimenez, J., Hawkins, B. L., and Maciel, G. E.**, Cross-polarization, magic-angle spinning <sup>13</sup>C nuclear magnetic resonance spectroscopy of soil humic fractions. *Org. Geochem.*, 9, 277, 1986.

79. Kan, R. I., Rubinsztain, Y., Ioselis, P., Aizenshtat, Z., Pugmire, R., Anderson, L. L., and Woolfenden, W. R., Carbon-13 Cross-polarized magic-angle sample spinning nuclear magnetic resonance of melanoidins. *Org. Geochem.*, 9, 199, 1986.
80. Earl, W. L., Wershaw, R. L., and Thorn, K. A., The use of variable temperature and magic-angle sample spinning in studies of fulvic acids. *J. Magn. Reson.*, 74, 264, 1987.
81. Preston, C. M. and Blackwell, B. A., Carbon-13 nuclear magnetic resonance for a humic and a fulvic acid: signal-to-noise optimization, quantitation, and spin-echo techniques. *Soil Sci.*, 139, 88, 1985.
82. Lobartini, J. C. and Tan, K. H., Differences in humic acid characteristics as determined by carbon-13 nuclear magnetic resonance, scanning electron microscopy, and infrared analysis. *Soil Sci. Soc. Am. J.*, 52, 125, 1988.
83. Theng, B. K. G., *The Chemistry of Clay-Organic Reactions*. Higler, London, 1974.
84. Theng, B. K. G., Churchman, G. J., and Newman, R. H., The occurrence of interlayer clay-organic complexes in two New Zealand soils. *Soil Sci.*, 142, 262, 1986.
85. Gerasimowicz, W. V., Hicks, K. B., and Pfeffer, P. E., Evidence for the existence of associated lignin-carbohydrate polymers as revealed by carbon-13 CPMAS solid-state NMR spectroscopy. *Macromolecules*, 17, 2597, 1984.
86. Atalla, R. H., Gast, J. C., Sindorf, D. W., Bartuska, V. J., and Maciel, G. E., Carbon-13 NMR spectra of cellulose polymorphs. *J. Am. Chem. Soc.*, 102, 3249, 1980.
87. Earl, W. L. and VanderHart, D. L., High resolution, magic angle spinning carbon-13 NMR of solid cellulose I. *J. Am. Chem. Soc.*, 102, 3251, 1980.
88. Robert, D. and Gagnaire, D., Quantitative analysis of lignins by carbon-13 NMR. *Int. Symp. Wood Pulping Chemistry*, 1, 86, 1981.
89. Earl, W. L. and VanderHart, D. L., Observations by high-resolution carbon-13 nuclear magnetic resonance of cellulose I related to morphology and crystal structure. *Macromolecules*, 14, 570, 1981.
90. Maciel, G. E., Kolodzieski, W., Bertran, M., and Dale, B., Carbon-13 NMR and order in cellulose. *Macromolecules*, 15, 686, 1982.
91. Horii, F., Hirai, A., and Kitamaru, R., Solid-state high-resolution carbon-13 NMR studies of regenerated cellulose samples with different crystallinities. *Polym. Bull.*, 8, 163, 1982.
92. Nimz, H. H. and Nemr, M., Carbon-13 NMR spectra of lignins. 9. Spin-lattice relaxation times (T1) and determination of interunit linkages in three hardwood lignins. (*Alnus glutinosa*, *Corylus avellanus* and *Acer pseudoplatanus*). *J. Wood Chem. Technol.*, 2, 371, 1982.
93. Kolodzieski, W., Frye, J. S., and Maciel, G. E., Carbon-13 nuclear magnetic resonance spectrometry with cross-polarization and magic-angle spinning for analysis of lodgepole pine wood. *Anal. Chem.*, 54, 1419, 1982.
94. Opella, S. J. and Frey, M. H., Selection of non-protonated carbon resonances in solid-state nuclear magnetic resonance. *J. Am. Chem. Soc.*, 101, 5854, 1979.
95. Opella, S. J., Frey, M. H., and Cross, T. A., Detection of individual carbon resonances in solid proteins. *J. Am. Chem. Soc.*, 101, 5856, 1979.
96. Alemany, L. B., Grant, D. M., Pugmire, R. J., Alger, T. D., and Zilm, K. W., Cross-polarization and magic angle sample spinning NMR spectra of model organic compounds. I. Highly protonated molecules. *J. Am. Chem. Soc.*, 105, 2133, 1983.
97. Alemany, L. B., Grant, D. M., Pugmire, R. J., Alger, T. D., and Zilm, K. W., Cross-polarization and magic angle sample spinning NMR spectra of model organic compounds. II. Molecules of low or remote protonation. *J. Am. Chem. Soc.*, 105, 2142, 1983.
98. Alemany, L. B., Grant, D. M., Alger, T. D., and Pugmire, R. J., Cross-polarization and magic angle sample spinning NMR spectra of model organic compounds. III. Effect of the <sup>13</sup>C-<sup>1</sup>H dipolar interaction on cross-polarization and carbon-proton dephasing. *J. Am. Chem. Soc.*, 105, 6697, 1983.
99. Ludemann, H.-D. and Nimz, H., Carbon-13 nuclear magnetic resonance spectra of lignins. *Biochem. Biophys. Res. Commun.*, 52, 1162, 1973.
100. Himmelsbach, D. S. and Barton, F. E., Carbon-13 nuclear magnetic resonance of grass lignins. *J. Agric. Food Chem.*, 28, 1203, 1980.
101. Sjostrom, E., *Wood Chemistry Fundamentals and Applications*. Academic Press, New York, 1981, 56.
102. Zumbulyadis, N., Selective carbon excitation and the detection of spatial heterogeneity in cross-polarization magic-angle spinning NMR. *J. Magn. Reson.*, 53, 486, 1983.
103. Gillam, A. H., Wilson, M. A., and Collin, P. J., Structural analysis of sea loch sedimentary humic substances by <sup>13</sup>C-<sup>1</sup>H dipolar dephasing NMR. *Org. Geochem.*, 11, 91, 1987.
104. Miknis, F. P., Lindner, A. W., Gannon, A. J., Davis, M. F., and Maciel, G. E., Solid-state <sup>13</sup>C-NMR studies of selected oil shales from Queensland, Australia. *Org. Geochem.*, 7, 239, 1984.
105. Wilson, M. A., Verheyen, T. V., Vassallo, A. M., Hill, R. S., and Perry, G. J., Selective loss of carbohydrates from plant remains during coalification. *Org. Geochem.*, 11, 265, 1987.
106. Williams, R. J. P., Giles, R. G. F., and Posner, A. A. M., Solid-state phosphorus NMR spectroscopy of minerals and soils. *J. Chem. Soc. Chem. Commun.*, 20, 1051, 1981.

107. **Frye, J. S., Bronnimann, C. E., and Maciel, G. E.,** Solid-state NMR of humic materials, in *NMR of Humic Substances and Coal*, Wershaw, W. L. and Mikita, M. A., Eds., Lewis Publishers, Chelsea, MI, 1987, 33.
108. **Turner, G. L., Smith, K. A., Kirkpatrick, R. J., and Oldfield, E.,** Structure and cation effects on phosphorus-31 NMR chemical shifts and chemical-shift anisotropies of orthophosphates, *J. Magn. Reson.*, 70, 408, 1986.
109. **Benzing-Purdie, L., Ripmeester, J. A., and Preston, C.,** Elucidation of the nitrogen forms in melanoidins and humic acid by nitrogen-15 cross-polarization magic angle spinning nuclear magnetic resonance spectroscopy, *J. Agric. Food Chem.*, 31, 913, 1983.
110. **Benzing-Purdie, L., Cheshire, M. V., Williams, B. L., Sparling, G. P., Ratcliffe, C. I., and Ripmeester, J. A.,** Fate of [<sup>15</sup>N] Glycine in peat as determined by <sup>13</sup>C and <sup>15</sup>N CP-MAS NMR spectroscopy, *Agric. Food Chem.*, 34, 170, 1986.
111. **Burum, D. P. and Rhim, W. K.,** Analysis of multiple pulse NMR in solids. III, *J. Chem. Phys.*, 71, 944, 1979.
112. **Pembleton, R. G., Ryan, L. M., and Gerstein, B. C.,** NMR probe for combined homonuclear multiple pulse decoupling and magic angle spinning, *Rev. Sci. Instrum.*, 48, 1286, 1977.
113. **Walter, T. W., Turner, G. L., and Oldfield, E.,** Oxygen-17 cross-polarization NMR spectroscopy of inorganic solids, *J. Magn. Reson.*, 76, 106, 1988.